Available online at www.sciencedirect.com
ScienceDirect
Comput. Methods Appl. Mech. Engrg. xxx (xxxx) xxx
Computer methods in applied mechanics and engineering
www.elsevier.com/locate/cma

Angles between subspaces and nearly optimal approximation in GFEM

Robert Lipton[a,*], Paul Sinz[b,c], Michael Stuebner[d]

[a] Department of Mathematics, LSU, Baton Rouge, LA, United States of America
[b] Lucido LLC, Lewisville, TX, United States of America
[c] Michigan State University, United States of America
[d] Global Engineering and Materials, Inc.„ Princeton, NJ, United States of America

Available online xxxx

Contribution for the Special Issue "A Special Issue in Honor of the Lifetime Achievements of J. Tinsley Oden"

Abstract

The Generalized Finite Element Methods (GFEM) are known for accurately resolving local features in heterogeneous media. Recent numerical experiments have shown that the use of local bases made from $\mathbb{A}$-harmonic extensions of well chosen boundary data have nearly optimal approximation properties. In this paper we show that the explanation is geometric and given by the angle between any finite dimensional approximation space and the optimal finite dimensional approximation space introduced in (Babŭska and Lipton, 2011). The effect of the angle is quantified by an upper bound on the convergence rate. This rate is seen in the numerical simulations where local bases with nearly optimal approximation properties are identified.

Keywords: Generalized Finite Element Methods; Local approximation spaces; Grassman angles

1. Introduction

Applications of science and technology increasingly require efficient methods for the numerical solution of multiscale heterogeneous problems. The primary challenge in these problems arises from the extreme degrees of freedom required to parameterize material heterogeneity. Multiscale numerical methods provide one way to solve large problems by employing local and independent computations that enable a global solve involving a drastically reduced number of degrees of freedom.

In this investigation we address the generalized finite element method (GFEM) introduced in [1] and extended in [2,3]. This approach is a partition of unity method (PUM) [4] which utilizes the results of many independent and local computations carried out across the computational domain $\Omega \subset \mathbb{R}^d$, $d = 2, 3$. The PUM is a domain decomposition methodology in which the computational domain is partitioned into an overlapping collection of preselected subsets ω_i, $i = 1, 2, \ldots, m$ (see Fig. 1). Here a finite-dimensional approximation space V_{ω_i} is constructed over each subset using local information in a two step procedure. In the first step local solutions to

* Corresponding author.
E-mail addresses: lipton@lsu.edu (R. Lipton), paul.sinz@gmail.com (P. Sinz), mstuebner@gem-innovation.com (M. Stuebner).
URL: http://www.math.lsu.edu/~lipton/ (R. Lipton).

https://doi.org/10.1016/j.cma.2022.115628
0045-7825/

Please cite this article as: R. Lipton, P. Sinz and M. Stuebner, Angles between subspaces and nearly optimal approximation in GFEM, Computer Methods in Applied Mechanics and Engineering (2022) 115628, https://doi.org/10.1016/j.cma.2022.115628.

the problem are solved over enlarged subdomains $\omega_i^* \supset \omega_i$ generating the finite dimensional space $V_{\omega_i^*}$. In the second step the solutions are restricted to the smaller set $\omega_i \subset \omega_i^*$. This way of generating the local basis V_{ω_i} is called oversampling. The oversampling method is motivated by the maximum principle for scalar problems and by the St. Venant principle for problems of elasticity [5]. It is a major feature of the multiscale finite element methods (MSFEM) introduced in [6–8]. In the GFEM scheme each subspace V_{ω_i} is computed independently. A global approximation space V^M over Ω is constructed by "pasting" together the local spaces with a partition of unity (e.g., [9]). For large problems, the resulting global system constructed with V^M is orders of magnitude smaller than the system resulting from a direct application of the finite element method (FEM) [10].

The accuracy of the method is controlled by the accuracy of the local approximations inside each subdomain [11]. As a consequence the overall computational complexity increases as efforts directed towards reducing the local approximation error are applied. One aims to strike an acceptable balance between the two competing demands of global accuracy and local computational efficiency. In this paper we address this problem by introducing local approximation spaces that provide both a reduction in computational complexity and maintain accuracy when compared to the optimal local basis associated with oversampling developed in [12].

The oversampling method for generating a local basis is illustrated for a generic domain ω^* interior to Ω. We first define an $\mathbb{A}$-harmonic function on $S \subset \Omega$ as an $H^1(S)$ function $u(\mathbf{x})$ satisfying

$$-\operatorname{div}(\mathbb{A}(\mathbf{x})\nabla u(\mathbf{x})) = 0, \qquad \mathbf{x} \text{ in } S \tag{1.1}$$

where $\mathbb{A}(x)$ is a given $L^\infty(S)$ coefficient satisfying $0 < \Lambda^{-1}|\mathbf{v}|^2 \leq \mathbb{A}\mathbf{v}\cdot\mathbf{v} \leq \Lambda|\mathbf{v}|^2$ for $\Lambda > 0$. In [12] the operator R given by the restriction of non-constant $\mathbb{A}$-harmonic functions defined on ω^* to ω is studied. The Hilbert space of non-constant $\mathbb{A}$-harmonic functions that are bounded in the energy norm $\|u\|_{\mathcal{E}(S)} := (\int_S \mathbb{A}\nabla u \cdot \nabla u \, d\mathbf{x})^{1/2}$ is denoted by $\mathcal{A}(S)$. Here $R : \mathcal{A}(\omega^*) \to \mathcal{A}(\omega)$. When ω^* lies in the interior of Ω and $\omega \subset\subset \omega^*$, the restriction operator is shown in [12] to be compact and has a countable number of singular values λ_M converging to zero as the index M goes to infinity. The eigenvalues are ordered according to max–min and the associated eigenspaces E_M are of finite dimension M and have optimal approximation properties over all $\mathbb{A}$-harmonic bases of the same dimension. The optimal relative approximation error in the energy norm over ω is given by $\sqrt{\lambda_{M+1}}$ with $\lambda_{M+1} \to 0$ (see Theorem 3.1). The relative approximation error on ω is shown in [12] to converge nearly exponentially to zero as $M \to \infty$. These approximation rates are with respect to the energy norm over ω. These results can be extended to subdomains ω that are adjacent to the boundary of the computational domain. For this case ω is not compactly contained in ω^* but is a subset of ω^* with homogeneous Neumann or Dirichlet data on shared boundaries of Ω (see Section 4). To achieve a relative error tolerance of τ the number of optimal local basis functions needed are $O(\log(1/\tau))^{d+1}$ [10]. An advantage is that these local approximation spaces can be computed offline and independently of local bases on other subdomains providing the opportunity for parallelization. This observation applies to elastic equilibrium problems as well [10]. However, for large three dimensional computations one seeks to further reduce the computational complexity of local calculations when possible.

One observes that the numerical construction of the optimal local basis requires the solution of an eigenvalue problem over the space of $\mathbb{A}$-harmonic functions. The optimal local approximation space is a subspace spanned by M eigenfunctions. Because of this one has to first construct a subspace generated by $\mathbb{A}$-harmonic functions of greater dimension $L > M$ and then use it to find the M eigenfunctions. On the other hand it would require less computational effort to simply use N linearly independent $\mathbb{A}$-harmonic functions as the approximation space where $M \leq N < L$. The question becomes which among the alternate $\mathbb{A}$-harmonic bases is to be used and what does its dimension N have to be in order to obtain a useful approximation.

With this goal in mind the computational experiments of [13] use the trace of harmonic polynomials on $\partial\omega^*$ as boundary data to generate $\mathbb{A}$-harmonic bases that deliver exponential convergence of errors in the preasymptotic regime for two-phase conductors. For problems of two-phase elasticity, $\mathbb{A}$-harmonic bases made using traces of tensor products of harmonic polynomials as boundary data are also shown to give exponential convergence in the energy norm [13]. More recently, boundary data given by trigonometric polynomials or triangle waves with increasing oscillation are used to generate bases of $\mathbb{A}$-harmonic functions that can approximate the local solution with exponential accuracy [9]. The earlier work of [14] use the trace of harmonic polynomials on $\partial\omega^*$ as boundary data for heat conduction in the presence of distributed voids and their numerical simulations deliver exponential decay of approximation error. Alternative approaches have employed randomly generated bases invoking the theory of randomized linear algebra to generate less expensive local bases with expected relative approximation error $\sqrt{M\lambda_{M+1}}$ [15,16].

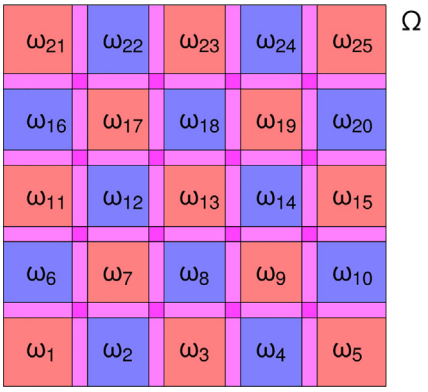

Fig. 1. Domain Ω with overlapping subdomains labeled here as ω_i, $i = 1, \ldots, 25$. The pink regions indicate where subdomains overlap. (For interpretation of the references to color in this figure legend, the reader is referred to the web version of this article.)

In this paper we are motivated by these studies and address this problem geometrically and compare the approximation properties of the M dimensional optimal local approximation space V^M with respect to an N-dimensional approximation space of $\mathbb{A}$-harmonic functions W^N defined on ω^*. In order to compare the approximation errors between spaces we introduce an approximation error for W^N given by its "Sup-Inf". The Sup-Inf is used as a tool for computing the relative error of approximation spaces see, e.g., [13,17]. This is defined in the following section. The spectral definition of Sup-Inf is used for the numerical calculations and is given in Section 5. The Sup-Inf for an N-dimensional space of $\mathbb{A}$-harmonic functions is denoted by $\sqrt{\mu_N}$. In this paper we examine the orientation between the finite dimensional subspaces V^M and W^N for $N \geq M$ and the approximation error made using the local subspace W^N. The orientation measure we use is a cosine of a special angle β_M^N between the N dimensional space and the M dimensional space defined by

$$\cos^2(\beta_M^N) := \inf_{e \in V^M} \frac{\left(\mathbb{P}_{W^N} e, e\right)_{\mathcal{E}(\omega^*)}}{\|e\|_{\mathcal{E}(\omega^*)}}. \tag{1.2}$$

The quantity $\cos^2(\beta_M^N)$ turns out to be related to $\cos^2(\Theta_M^N)$ where Θ_M^N is the Grassmann angle between the two subspaces [18]. These angles can be computed numerically and appear in other areas of approximation theory [19,20] (see Section 3.1). We show that if we choose the approximation space appropriately the cosine of β_M^N and the cosine of Θ_M^N become greater than zero simultaneously and we can use the less computationally intensive basis to approximate any $\mathbb{A}$-harmonic function in $H^1(\omega^*)$ restricted to ω nearly as well as the optimal basis. We quantify this statement by explicitly relating the angle between subspaces to the approximation error of the simpler $\mathbb{A}$-harmonic space. The principle result of this paper is now described here and again in Section 3.1 where it is proved. We fix $0 < \alpha < 1$ and define $N^\alpha(M)$ to be the smallest integer $N \geq M > 0$ for which

$$\cos^2(\beta_M^N) = \alpha > 0.$$

Then when $\beta_M^N \in (0, \pi/2]$ the relative approximation error associated with the local approximation space W^N, as measured in the energy norm over ω, is less than

$$\sqrt{\lambda_{M+1}}(1 + (\cos \beta_M^N)^{-1}), \tag{1.3}$$

when N is equal to $N^\alpha(M)$. For properly chosen bases, including the $\mathbb{A}$-harmonic extension of trigonometric boundary data, the numerical examples given in Section 7 (e.g., Fig. 12) show for $\alpha = 0.4$ and $\omega \subset \omega^*$, where ω^* has twice the side length of ω, that $M \leq N^\alpha(M) \leq M + 10$. We numerically examine the effect of contrast and degree of oversampling on the behavior of $\cos \beta_M^N$ with respect to N for fixed M in Section 7.

Numerical strategies for reducing computational work through the use of local bases has been explored extensively in the literature. One way to address multiscale computation is to exploit the local periodicity or stochastisicity of a microstructure and make use of homogenization theory [21]. These methods include the original Multiscale FEM [6] and the variational multiscale method [22]. In the absence of local structure one can consider

approaches to numerical homogenization for rough coefficients (i.e., L^∞ coefficients). However, the lack of local structure naturally degrades the efficiency and convergence rates. Nonetheless, the size of the global solve can be reduced and several methods have been proposed for L^∞ coefficients that offer significant dimension reduction. There are a variety of methods including upscaling based on harmonic coordinates and elliptic inequalities [23,24], elliptic solvers based on H-matrices [25,26], explicit solution of local computations through Bayesian numerical homogenization [27], dimension reduction methods based on global changes of coordinates and MSFEM for upscaling porous media flows [28,29], the heterogeneous multiscale methods [30–32], an adaptive coarse scale–fine scale projection method [33], subgrid upscaling methods [34], and global Galerkin projection schemes for problems with L^∞ coefficients and homogeneous Dirichlet boundary data [35]. More recent developments include numerical homogenization based on the flux norm for L^∞ coefficients [36], rough polyharmonic splines [37], new MSFEM methods [38], and static condensation using optimal local basis [39]. For a coarse mesh of diameter H local bases that deliver order H convergence with $O(\log(1/H))^{d+1}$ approximation functions are developed in [40]. For comparison, the method presented here and in [10,12] shows that the coarse mesh can be fixed arbitrarily and for a given relative error τ one needs $O(\log(1/\tau))^{d+1}$ "n-width" approximation functions.

The paper is organized as follows: The next section provides a brief review of the GFEM. The subsequent Section 3 provides the main theorems and proofs on local approximation using angles between finite dimensional subspaces. Section 4 extends the ideas to subdomains that are adjacent to the boundary. A spectral characterization for the Sup-Inf is given in Section 5. Section 6 provides the approximation results in the finite dimensional context. The numerical simulations are carried out in Section 7. Conclusions are given in Section 8.

2. Outline of the GFEM

To fix ideas we consider the boundary value problem over bounded domain $\Omega \subset \mathbb{R}^d$ with piecewise C^1-boundary given by

$$-\operatorname{div}(\mathbb{A}(\mathbf{x})\nabla u(\mathbf{x})) = f(\mathbf{x}),\ \ \mathbf{x} \in \Omega \tag{2.1}$$

with Neumann boundary conditions on $\partial\Omega$

$$\mathbf{n} \cdot \mathbb{A}(\mathbf{x})\nabla u(\mathbf{x}) = g(\mathbf{x}),\ \mathbf{x} \in \partial\Omega, \tag{2.2}$$

where $\mathbf{n}$ is the unit outer normal vector. The data satisfies the consistency condition

$$\int_{\partial\Omega} g\, d\mathbf{x} + \int_{\Omega} f\, dx = 0.$$

Here $\mathbb{A}(\mathbf{x})$ is the $d \times d$ conductivity matrix with rough coefficients $\mathbb{A}_{ij}(\mathbf{x}) \in L^\infty(\Omega)$ given in the introduction.

The weak solution $u \in H^1(\Omega)$ of (2.1) satisfies

$$(u, v)_{\mathcal{E}(\Omega)} = F(v) \tag{2.3}$$

for all $v \in H^1(\Omega)$ where

$$(u, v)_{\mathcal{E}(\Omega)} = \int_{\Omega} \mathbb{A}(\mathbf{x})\nabla u \cdot \nabla v\, d\mathbf{x} \text{ and } F(v) = \int_{\Omega} f v\, d\mathbf{x} + \int_{\partial\Omega} g v\, ds.$$

It is pointed out that there is nothing special to the Neumann boundary value problem and the Dirichlet boundary value problem can be considered as well. Here $u(\mathbf{x}) = h(\mathbf{x})$ for $\mathbf{x} \in \partial\Omega$, where $h(\mathbf{x})$ is the Dirichlet data. For future reference we define the semi-norm $(u, u)_{\mathcal{E}(\Omega)} = \|u\|_{\mathcal{E}(\Omega)}$ which becomes a norm on the quotient space $H^1(\Omega)/\mathbb{R}$.

2.1. The GFEM approximation scheme

The GFEM is a domain decomposition method. Over each subdomain a local approximation is generated by a linear combination of two functions one coming from a local finite dimensional space of $\mathbb{A}$-harmonic functions and the other being a local particular solution. In this version of GFEM the local $\mathbb{A}$-harmonic subspace is obtained using oversampling. The computations associated with the construction of different local approximation spaces are independent and can be performed in parallel. This is also true for the local particular solutions. When using the optimal local $\mathbb{A}$-harmonic bases the resulting global stiffness matrix can be several orders of magnitude smaller than the stiffness matrix obtained by applying FEM directly [10].

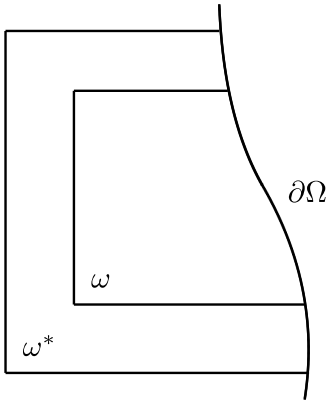

Fig. 2. Subdomain ω and extended subdomain ω^* adjacent to the boundary $\partial\Omega$.

We now describe the partition of unity. Let $\{\omega_i\}_{i=1}^m$ be a collection of open sets covering the domain Ω such that $\cup_{i=1}^N \omega_i = \Omega$ and let $\phi_i \in C^1(\omega_i)$, $i = 1, \ldots, m$, be a partition of unity subordinate to the open covering. The partition of unity functions satisfy the following properties:

$$
\begin{aligned}
&0 \le \phi_i \le 1, \quad i = 1, \ldots, N,\\
&\phi_i(x) = 0,\ x \in \Omega\backslash\omega_i, \quad i = 1, \ldots, N,\\
&\sum_i \phi_i(x) = 1 \quad \forall x \in \Omega,\\
&\max_{x\in\Omega} |\phi_i(x)| \le C_1, \quad i = 1, \ldots, N,\\
&\max_{x\in\Omega} |\nabla\phi_i(x)| \le \frac{C_2}{\mathrm{diam}(\omega_i)}, \quad i = 1, \ldots, N,
\end{aligned}
$$

where C_1 and C_2 are bounded positive constants and $\mathrm{diam}(\omega_i)$ is the diameter of the set ω_i. The partition of unity functions can be chosen to be flat-topped so that local approximation spaces are linearly independent and for ensuring good conditioning of the global stiffness matrix [41,42]. Let $\{\omega_i^*\}_{i=1}^N$ be a second covering such that each ω_i is contained within the larger open set ω_i^*. For ω_i in the interior of Ω we have ω_i^* in the interior and $\mathrm{dist}(\partial\omega_i^*, \partial\omega_i) > 0$. When ω_i is adjacent to the boundary $\partial\Omega$ then ω_i^* also has boundary parts in common with $\partial\Omega$. We drop the indices for convenience and let $\partial\omega_b^*$ denote the part of the boundary of ω^* in common with $\partial\Omega$ defined by $\partial\omega_b^* = \partial\Omega \cap \partial\omega^*$ and define $\partial\omega_b = \partial\Omega \cap \partial\omega$. The remaining boundary parts of $\partial\omega^*$ and $\partial\omega$ are interior to Ω and denoted by $\partial\omega_I$ and $\partial\omega_I^*$. We enforce $\mathrm{dist}(\partial\omega_I^*, \partial\omega_I) > 0$ (see Fig. 2).

The local approximations are separated into local particular solutions and a local approximation space $V_{\omega_i^*}^{m_i}$ of dimension m_i. Here $V_{\omega_i^*}^{m_i} = W^{m_i-1} + c_i$, where $W^{m_i-1} \subset \mathcal{A}(\omega^*)$ is a $m_i - 1$ dimensional non-constant $\mathbb{A}$-harmonic approximation space and c_i is an arbitrary constant on ω_i^* independent of the constants on other subdomains. For domains adjacent to the boundary, the local $\mathbb{A}$-harmonic space is further restricted to the space of $\mathbb{A}$-harmonic functions that satisfy homogeneous Neumann conditions on $\partial\omega_b^*$. The global approximation space is constructed from the local approximation spaces and is defined by

$$
V^N = \left\{ \sum_{i=1}^N \phi_i \xi_i : \xi_i \in V_{\omega_i^*}^{m_i} \right\}. \tag{2.4}
$$

The local particular solution over ω_i^* solves the inhomogeneous problem

$$
-\mathrm{div}(\mathbb{A}(\mathbf{x})\nabla\chi_i(\mathbf{x})) = f(\mathbf{x}),\ x \in \omega_i^* \tag{2.5}
$$

with $\chi_i \in H_0^1(\omega_i^*)$ if ω_i^* lies on the interior of Ω, or, for ω_i^* adjacent to $\partial\Omega$, the particular solution $\chi_i \in H^1(\omega_i^*)$ satisfies $\mathbf{n} \cdot \mathbb{A}(\mathbf{x})\nabla\chi_i(\mathbf{x}) = g$ on $\partial\omega_i^* \cap \partial\Omega$ and $\mathbf{n} \cdot \mathbb{A}(\mathbf{x})\nabla\chi_i(\mathbf{x}) = 0$ on $\partial\omega_i^* \cap \Omega$. The global particular solution u^F

is defined as

$$u^F = \sum_{i=1}^{N} \phi_i \chi_i. \tag{2.6}$$

The global solution is posed over the convex space $K^N = V^N + u^F$. This problem is a variational inequality over the convex space K^N. Here we seek a solution $u^H \in V^N(\Omega)$ to the following problem for all $v \in V^N$

$$(u^H, v)_{\mathcal{E}(\Omega)} = F(v) - (u^F, v)_{\mathcal{E}(\Omega)}. \tag{2.7}$$

The GFEM solution is given by $u^G = u^H + u^F$. The existence of a unique solution $u^G \in K^N$ follows from the theory of variational inequalities (e.g., [43]). In the GFEM scheme the local error explicitly controls the global error. If the local errors, as measured by the energy norms over ω_i, are bounded by ϵ_i, $i = 1, \ldots, N$, then the global error over Ω is bounded by

$$\|u - u_G\|_{\mathcal{E}(\Omega)} \leq \kappa^{1/2} C \left(\sum_{i}^{N} \epsilon_i^2 \right)^{1/2} \|u\|_{\mathcal{E}(\Omega)}. \tag{2.8}$$

This is established in [44] and the proof adapted for the case treated here can be found in [9]. Here C depends on Λ and κ depends on the partition of unity. In the next section we focus on the reduction of the local approximation errors while at the same time minimizing the computational complexity of constructing the local approximations.

3. Geometry in Hilbert space and approximation

In this section we quantify the ability of simpler finite dimensional local approximation spaces to provide approximation error comparable to the optimal local approximation in terms of the angle between the two subspaces. We consider subdomains ω belonging to the covering $\Omega = \cup_j \omega_i$ that are interior to Ω. In the next section we show how to handle the case when ω is not an interior subdomain. When ω is interior to Ω we can find a bigger open set ω^* compactly contained in Ω that also compactly contains ω.

We now demonstrate the construction of the class of finite dimensional subspaces of $\mathcal{A}(\omega^*)$. We introduce a countable set of functions $\{f_i\}_{i=1}^{\infty}$ on the boundary $\partial\omega^*$ that form a dense system in $H^{1/2}(\partial\omega^*)$. Examples of such systems are common and given by the boundary traces of the Stekloff eigenfunctions, the traces of Neumann eigenfunctions on $\partial\omega^*$, and systems of progressively finer finite dimensional FEM basis for $H^{1/2}(\partial\omega^*)$. We choose a system of N linearly independent functions defined on $\partial\omega^*$ and extend these to the interior of ω^* as $\mathbb{A}$-harmonic functions w_i by finding the $H^1(\omega^*)$ solution w_i of

$$-\operatorname{div}(\mathbb{A}(\mathbf{x})\nabla w_i(\mathbf{x})) = 0, \qquad \mathbf{x} \text{ on } \omega^* \tag{3.1}$$

with boundary values $w_i = f_i \in H^{1/2}(\partial\omega^*)$. These functions form a basis for an N-dimensional subspace of $\mathcal{A}(\omega^*)$. We denote this subspace by $W^N = \operatorname{span}\{w_1, w_2 \ldots, w_N\}$.

Now we construct finite dimensional subspaces of $\mathcal{A}(\omega^*)$ with optimal approximation properties on ω. Consider the restriction of functions in $\mathcal{A}(\omega^*)$ to ω. The restriction operator $R : \mathcal{A}(\omega^*) \to \mathcal{A}(\omega)$ is a compact operator [12]. The eigenvalues λ_j of R^*R decrease monotonically to zero with the index $j \to \infty$. We define $\{e_j\}_{j=1}^{\infty} \subset \mathcal{A}(\omega^*)$ to be the associated eigenfunctions given by

$$R^*Re_j = \lambda_j e_j, \tag{3.2}$$

or

$$(e_j, v)_{\mathcal{E}(\omega)} = \lambda_j (e_j, v)_{\mathcal{E}(\omega^*)}, \tag{3.3}$$

for all $v \in \mathcal{A}(\omega^*)$. Here we take the normalization $(e_i, e_j)_{\mathcal{E}(\omega^*)} = \delta_{ij}$. The eigenvalues $\{\lambda_n\}_{n=1}^{\infty}$ form a decreasing sequence of positive real numbers and we order the eigenvalues according to max–min. The space spanned by M eigenfunctions corresponding to the eigenvalues $\{\lambda_n\}_{n=1}^{M}$ is known to have optimal approximation properties. This is expressed in the following theorem from [12].

Theorem 3.1 (*Optimal Approximation Property*). *Given* $V^M = \operatorname{span}\{e_1, \ldots, e_M\}$ *and consider any* M *dimensional subspace* $W^M \subset \mathcal{A}(\omega^*)$ *then*

$$\sqrt{\lambda_{M+1}} = \sup_{u \in \mathcal{A}(\omega^*)} \inf_{e \in V^M} \frac{\|u - e\|_{\mathcal{E}(\omega)}}{\|u\|_{\mathcal{E}(\omega^*)}} = \inf_{W^M \subset \mathcal{A}(\omega^*)} \sup_{u \in \mathcal{A}(\omega^*)} \inf_{v \in W^M} \frac{\|u - v\|_{\mathcal{E}(\omega)}}{\|u\|_{\mathcal{E}(\omega^*)}}. \tag{3.4}$$

3.1. Approximation

The best relative approximation error of a function $u \in \mathcal{A}(\omega^*)$ over ω by an element of a subspace $W^N \subset \mathcal{A}(\omega^*)$ of dimension N is given by the "Sup-Inf",

$$\sqrt{\mu_N} = \sup_{u\in\mathcal{A}(\omega^*)} \inf_{v\in W^N} \frac{\|u-v\|_{\mathcal{E}(\omega)}}{\|u\|_{\mathcal{E}(\omega^*)}}. \tag{3.5}$$

A spectral characterization for the Sup-Inf is given in Section 5. The spectral characterization provides a means for computing the Sup-Inf numerically.

For a fixed M the optimal subspace V^M is seen to be given by the span of $\{e_j\}_{j=1}^M$ with

$$\sqrt{\lambda_{M+1}} = \sup_{u\in\mathcal{A}(\omega^*)} \inf_{e\in V^M} \frac{\|u-e\|_{\mathcal{E}(\omega)}}{\|u\|_{\mathcal{E}(\omega^*)}} \leq \sqrt{\mu_M}. \tag{3.6}$$

We introduce the relevant angle between the finite dimensional subspaces. First set $A_{ij} = (e_i, w_j)_{\mathcal{E}(\omega^*)}$. Let $V^M = \text{span}\{e_1, \ldots, e_M\}$ of the eigenfunctions of R^*R for which the approximation error is $\sqrt{\lambda_{M+1}}$ and $W^N = \text{span}\{w_1, \ldots, w_N\}$. With this choice A_{ij} is an $M \times N$ matrix. Let $\mathbb{P}_{W^N}$ be the orthogonal projection operator from $\mathcal{A}(\omega^*)$ into W^N, then a straight forward calculation (see the Appendix) shows that

$$\cos^2(\beta_M^N) := \inf_{e\in V^M} \frac{\left(\mathbb{P}_{W^N} e, e\right)_{\mathcal{E}(\omega^*)}}{\|e\|_{\mathcal{E}(\omega^*)}} = \lambda_{MIN}(AA^T) \tag{3.7}$$

where $\lambda_{MIN}(AA^T)$ is the smallest eigenvalue of AA^T. The angle β_M^N appearing in (3.7) is related to the square cosine of the Grassman angle Θ_M^N between the two subspaces [18]

$$\cos^2(\Theta_M^N) := \det\{AA^T\}, \tag{3.8}$$

so $\cos^2(\beta_M^N) = \cos^2(\Theta_M^N) = 0$ when $\lambda_{MIN}(AA^T) = 0$.

Theorem 3.2. *Given W^N, suppose $N \geq M$ and if $V^M \subset W^N$ then*

$$\sqrt{\mu_N} = \sup_{u\in\mathcal{A}(\omega^*)} \inf_{v\in W^N} \frac{\|u-v\|_{\mathcal{E}(\omega)}}{\|u\|_{\mathcal{E}(\omega^*)}} \leq \sqrt{\lambda_{M+1}}. \tag{3.9}$$

Note that with the hypothesis of Theorem 3.2 we have $\cos^2(\beta_M^N) = 1$.

Proof. Recall the hypothesis $N \geq M$ and if $V^M \subset W^N$ where V^M is the span of the first M optimal basis functions. Then given $u \in \mathcal{A}(\omega^*)$ since

$$\inf_{v\in W^N} \frac{\|u-v\|_{\mathcal{E}(\omega)}}{\|u\|_{\mathcal{E}(\omega^*)}} \leq \inf_{v\in V^M} \frac{\|u-v\|_{\mathcal{E}(\omega)}}{\|u\|_{\mathcal{E}(\omega^*)}} = \sqrt{\lambda_{M+1}}, \tag{3.10}$$

and the theorem follows from the definition of $\sqrt{\mu_N}$. □

The following corollary provides upper and lower bounds on the Sup-Inf.

Corollary 3.3. *If $N \geq M$ and $V^M \subset W^N$ then*

$$\sqrt{\lambda_{N+1}} \leq \sqrt{\mu_N} \leq \sqrt{\lambda_{M+1}} \tag{3.11}$$

Remark 3.4. The geometric requirement $\cos(\beta_M^N) > 0$ indicates that every n-width eigenfunction e_i, $i = 1, \ldots, M$ is not perpendicular to W^N.

The criterion e_i is not perpendicular to W^N, $i = 1, \ldots, N$ is necessary for $\sqrt{\mu_N} \leq \sqrt{\lambda_{M+1}}$.

Theorem 3.5. *Given $N \geq M$ suppose*

$$\sqrt{\mu_N} \leq \sqrt{\lambda_{M+1}}, \tag{3.12}$$

then

$$\mathrm{e}_i \not\perp W^N, \ i = 1, \ldots, M. \tag{3.13}$$

Proof. We prove this theorem by contradiction. Assume that $\mu(N) \leq \sqrt{\lambda_{M+1}}$ and there is a $e_i \in V^M$ such that e_i is perpendicular to W^N for some $i \in \{1, 2, \ldots, M\}$. Choose $u \in \mathcal{A}(\omega^*)$ of the from $u = ce_i$ where c is a scalar. So u is perpendicular to W^N in the $(\cdot,\cdot)_{\mathcal{E}(\omega^*)}$ inner product. It also follows from (3.3) that u is perpendicular to W^N in the $(\cdot,\cdot)_{\mathcal{E}(\omega)}$ inner product, so for any $v \in W^N$ we have

$$\begin{aligned} \|u - v\|^2_{\mathcal{E}(\omega)} &= \|u\|^2_{\mathcal{E}(\omega)} + \|v\|^2_{\mathcal{E}(\omega)} \\ &> \|u\|^2_{\mathcal{E}(\omega)} = \lambda_i \|u\|^2_{\mathcal{E}(\omega^*)} \\ &\geq \lambda_M \|u\|^2_{\mathcal{E}(\omega^*)}. \end{aligned} \tag{3.14}$$

It is evident from (3.14) that $\sqrt{\lambda_M} < \mu(N) \leq \sqrt{\lambda_{M+1}}$ and we arrive at the contradiction since $\sqrt{\lambda_{M+1}} < \sqrt{\lambda_M}$. □

A direct implication of Theorem 3.5 is the corollary,

Corollary 3.6. *Given $N \geq M$ suppose there is an i for which $e_i \perp W^N$ then*

$$\sqrt{\lambda_{M+1}} < \sqrt{\mu_N}. \tag{3.15}$$

Definition 3.7. Given $\alpha > 0$ and M fixed we define $N^\alpha(M)$ to be the smallest N such that $N \geq M$ for which

$$\cos^2(\beta_M^N) = \alpha > 0. \tag{3.16}$$

With this definition of $N^\alpha(M)$ we express the approximation error incurred using the subspace W^N.

Theorem 3.8. *Given M suppose $\beta_M^N \in (0, \pi/2]$ with $\cos \beta_M^N = \sqrt{\alpha} > 0$. For fixed α there exists an $N^\alpha(M)$ and*

$$\sqrt{\mu_{N^\alpha(M)}} = \sup_{u \in \mathcal{A}(\omega^*)} \inf_{v \in W^{N^\alpha(M)}} \frac{\|u - v\|_{\mathcal{E}(\omega)}}{\|u\|_{\mathcal{E}(\omega^*)}} \leq \sqrt{\lambda_{M+1}}(1 + (\cos \beta_M^N)^{-1}), \tag{3.17}$$

where $N^\alpha(M)$ increases monotonically with M.

This theorem quantifies the ability of a subspace to approximate an element $u \in \mathcal{A}(\omega^*)$ over $\omega \subset \omega^*$ in terms of its orientation to the optimally approximating subspace. In Section 7 we apply this inequality to corroborate the very good approximation properties of oversampled $\mathbb{A}$-harmonic bases used in numerical approximation for GFEM.

The proof of Theorem 3.8 is facilitated by the following lemma.

Lemma 3.9. *Suppose $\cos^2(\beta_M^N) > 0$ then for any $u \in \mathcal{A}(\omega^*)$ there exists a $v \in W^N$ such that $\mathbb{P}_{V^M}(v) = \mathbb{P}_{V^M}(u)$ and*

$$\|u - v\|_{\mathcal{E}(\omega)} \leq \sqrt{\lambda_{M+1}} \|u - v\|_{\mathcal{E}(\omega^*)} \tag{3.18}$$

We prove Lemma 3.9.

Proof. Given $h \in \mathcal{A}(\omega^*)$ and we have $h = \sum_{i=1}^\infty (e_i, h)_{\mathcal{E}(\omega^*)} e_i$ so the restriction operator $Rh = h|_\omega$ is given by

$$Rh = \sum_{i=1}^\infty (e_i, h)_{\mathcal{E}(\omega^*)} Re_i \qquad Re_i = e_i|_\omega, \tag{3.19}$$

and from (3.3) $\|e_i\|_{\mathcal{E}(\omega)} = \lambda_i$, thus

$$\|Rh\|_{\mathcal{E}(\omega)} = \sqrt{\sum_{i=1}^\infty (e_i, h)^2_{\mathcal{E}(\omega)^*} \|e_i\|^2_{\mathcal{E}(\omega)}} = \sqrt{\sum_{i=1}^\infty \lambda_i (e_i, h)^2_{\mathcal{E}(\omega^*)}}. \tag{3.20}$$

So for $u \in \mathcal{A}(\omega^*)$ and $v \in W^N \subset \mathcal{A}(\omega^*)$ we set $h = u - v$ and apply (3.20)

$$\frac{\|R(u - v)\|^2_{\mathcal{E}(\omega)}}{\|u\|_{\mathcal{E}(\omega^*)}} = \frac{\|u - v\|^2_{\mathcal{E}(\omega)}}{\|u\|_{\mathcal{E}(\omega^*)}} = \frac{\sum_{i=1}^\infty \lambda_i (e_i, u - v)^2_{\mathcal{E}(\omega^*)}}{\|u\|_{\mathcal{E}(\omega^*)}} \tag{3.21}$$

From its definition $W^N = span\{w_1, \ldots, w_N\}$ and observe that for $v = \sum_{i=1}^N c_j w_j$, with $c_1, \ldots, c_n$ real numbers one has

$$\sum_{i=1}^{\infty} \lambda_i (e_i, u - v)^2_{\mathcal{E}(\omega^*)} = \sum_{i=1}^{\infty} \lambda_i |(e_i, u)_{\mathcal{E}(\omega^*)} - \sum_{j=1}^{N} c_j (e_i, w_j)_{\mathcal{E}(\omega^*)}|^2. \tag{3.22}$$

Next we show that we can find numbers $c_1, \ldots, c_N$ such that

$$(e_i, u)_{\mathcal{E}(\omega^*)} = \sum_{j=1}^{N} c_j (e_i, w_j)_{\mathcal{E}(\omega^*)}, \tag{3.23}$$

for $i = 1 \cdots M$. Note first that Eq. (3.23) can be written as $\sum_{j=1}^N A_{ij} c_j = f_i$ for $i = 1, \ldots, M$, where $f_i = (e_i, u)_{\mathcal{E}(\omega^*)}$. We write this in matrix vector notation as $A\vec{c} = \vec{f}$. To find $\vec{c}$ we look for $\vec{c}$ of the form $\vec{c} = A^T \vec{x}$ for $\vec{x} \in \mathbb{R}^M$ and it follows that $AA^T \vec{x} = \vec{f}$. Now $\lambda_{MIN}(AA^T) = \cos^2(\beta_M^N) > 0$ so AA^T inverse exists and inverting gives $\vec{x} = [AA^T]^{-1} \vec{f}$ and

$$\vec{c} = A^T [AA^T]^{-1} \vec{f}. \tag{3.24}$$

For this choice of c_j we apply (3.21), (3.22), (3.23) to get

$$\begin{aligned} \|u - v\|^2_{\mathcal{E}(\omega)} &\leq \lambda_{M+1} \sum_{i=M+1}^{\infty} |(e_i, u)_{\mathcal{E}(\omega^*)} - \sum_{j=1}^{N} c_j (e_i, w_j)_{\mathcal{E}(\omega^*)}|^2 \\ &\leq \lambda_{M+1} \sum_{i=M+1}^{\infty} (e_i, u - v)^2_{\mathcal{E}(\omega^*)} \\ &\leq \lambda_{M+1} \|u - v\|^2_{\mathcal{E}(\omega^*)}, \end{aligned} \tag{3.25}$$

and (3.18) is established. To show $\mathbb{P}_{V^M}(v) = \mathbb{P}_{V^M}(u)$ multiply both sides of (3.23) by e_i, sum over i and note $\mathbb{P}_{V^M}(r) = \sum_{i=1}^M (e_i, r)_{\mathcal{E}(\omega^*)} e_i$. □

We now prove Theorem 3.8

Proof. Given $u \in \mathcal{A}(\omega^*)$ from Lemma 3.9 there exists a $v \in W^N$ such that $\mathbb{P}_{V^M}(v) = \mathbb{P}_{V^M}(u)$ and

$$\begin{aligned} \|u - v\|_{\mathcal{E}(\omega)} &\leq \sqrt{\lambda_{M+1}} \|u - v\|_{\mathcal{E}(\omega^*)} \\ &\leq \sqrt{\lambda_{M+1}} \left(\|u\|_{\mathcal{E}(\omega^*)} + \|v\|_{\mathcal{E}(\omega^*)} \right). \end{aligned} \tag{3.26}$$

We estimate $\|v\|_{\mathcal{E}(\omega^*)}$. From $v = \sum_{j=1}^{N^\alpha} c_j w_j$ and orthonormality of $\{w_j\}_{j=1}^{N^\alpha}$ we get $\|v\|_{\mathcal{E}(\omega^*)} = |\vec{c}|$. Similarly $|\vec{f}| = \|\mathbb{P}_{V^M} u\|_{\mathcal{E}(\omega^*)}$. From (3.24) a straightforward calculation gives

$$\|v\|_{\mathcal{E}(\omega^*)} = |\vec{c}| = \sqrt{(AA^T)^{-1} \vec{f} \cdot \vec{f}} \leq \lambda_{MIN}^{-1/2}(AA^T) \|u\|_{\mathcal{E}(\omega^*)} = (\cos \beta_M^N)^{-1} \|u\|_{\mathcal{E}(\omega^*)}, \tag{3.27}$$

and we recover

$$\|u - v\|_{\mathcal{E}(\omega)} \leq \sqrt{\lambda_{M+1}} (1 + (\cos \beta_M^N)^{-1}) \|u\|_{\mathcal{E}(\omega^*)}. \qquad \square \tag{3.28}$$

4. Subdomains adjacent to the boundary

The results of the previous section apply verbatim to subdomains ω adjacent to the computational boundary $\partial\Omega$. The only adjustment is in the choice of optimal basis V^M and $\mathbb{A}$ harmonic basis W^N. Elements of the partition of unity adjacent to the boundary have boundary parts in common with $\partial\Omega$. Because of this we modify the definition of ω, see Fig. 2 as well as introduce spaces of $\mathbb{A}$ harmonic functions with homogeneous boundary data. As before $\omega \subset \omega^*$ but ω^* also has boundary parts in common with $\partial\Omega$. Let $\partial\omega_b^*$ denote the boundary parts of ω^* common to $\partial\Omega$ defined by $\partial\omega_b^* = \partial\Omega \cap \partial\omega^*$ and define $\partial\omega_b = \partial\Omega \cap \partial\omega$. The remaining boundary parts of $\partial\omega^*$ and $\partial\omega$ are interior to Ω and denoted by $\partial\omega_I$ and $\partial\omega_I^*$. We require $\text{dist}(\partial\omega_I^*, \partial\omega_I) > 0$, see Fig. 2. When Neumann data is prescribed on the boundary we handle this as in [9] by considering local particular $\mathbb{A}$-harmonic solutions v on ω^* with Neumann boundary data given on $\partial\omega_b^*$ and $v = 0$ on $\partial\omega_I^*$. Now define $H_n^1(\omega^*)$ to be all $H^1(\omega^*)$ functions with

$n \cdot \mathbb{A}\nabla u = 0$ on $\partial\omega_b^*$ and define $H_n^1(\omega)$ to be all $H^1(\omega)$ functions with $n \cdot \mathbb{A}\nabla u = 0$ on $\partial\omega_b$ where n is the outward directed unit normal to Ω. The $\mathbb{A}$-harmonic spaces are chosen as all $\mathbb{A}$-harmonic functions in $H_n^1(\omega^*)$ restricted to $H_n^1(\omega)$ and denoted by $\mathcal{A}_n(\omega^*)$ and $\mathcal{A}_n(\omega)$ respectively.

Similarly when Dirichlet data is prescribed on $\partial\Omega$ we handle as in [9] by considering local particular $\mathbb{A}$-harmonic solutions v on ω^* with Dirichlet boundary data given on $\partial\omega_b^*$ and $n \cdot \mathbb{A}\nabla v = 0$ on $\partial\omega_I^*$. Now define $H_d^1(\omega^*)$ as all $H^1(\omega^*)$ functions with $u = 0$ on $\partial\omega_b^*$ and define $H_d^1(\omega)$ as all $H^1(\omega)$ functions with $u = 0$ on $\partial\omega_b$. The corresponding $\mathbb{A}$-harmonic spaces are chosen as all $\mathbb{A}$-harmonic functions in $H_d^1(\omega^*)$ restricted to $H_d^1(\omega)$ and denoted by $\mathcal{A}_d(\omega^*)$ and $\mathcal{A}_d(\omega)$.

Next the class of simple finite dimensional subspaces of $\mathcal{A}_n(\omega^*)$ and $\mathcal{A}_d(\omega^*)$ are constructed. We begin describing finite dimensional subspaces of $\mathcal{A}_n(\omega^*)$. We introduce a countable set of functions $\{f_i\}_{i=1}^{\infty}$ on the boundary $\partial\omega_I^*$ that form a dense system in $H^{1/2}(\partial\omega_I^*)$ and order the basis in terms of increasing boundary oscillation. We choose a system of N linear independent functions defined on $\partial\omega_I^*$ numbered in order of increasing oscillation and extend these inside as $\mathbb{A}$-harmonic functions w_i by finding the $H^1(\omega^*)$ solution w_i of

$$-\operatorname{div}(\mathbb{A}(\mathbf{x})\nabla w_i(\mathbf{x})) = 0, \qquad \mathbf{x} \text{ on } \omega^* \tag{4.1}$$

with boundary values $w_i = f_i \in H^{1/2}(\partial\omega_I^*)$ and $n \cdot \mathbb{A}\nabla w_i = 0$ on $\partial\omega_b^*$. These functions form a basis for an N-dimensional subspace of $\mathcal{A}_n(\omega^*)$. We denote this subspace by $W_n^N = \operatorname{span}\{w_1, w_2 \ldots, w_N\}$.

To generate finite dimensional subspaces of $\mathcal{A}_d(\omega^*)$ we introduce a countable set of functions $\{f_i\}_{i=1}^{\infty}$ on the boundary $\partial\omega_I^*$ that form a dense system in $H_{00}^{1/2}(\partial\omega_I^*)$ (e.g., see page 31 of [45]) and order the basis in terms of increasing boundary oscillation. We choose a system of N linear independent functions defined on $\partial\omega_I^*$ numbered in order of increasing oscillation and extend these inside as $\mathbb{A}$-harmonic functions w_i by finding the $H^1(\omega^*)$ solution w_i of

$$-\operatorname{div}(\mathbb{A}(\mathbf{x})\nabla w_i(\mathbf{x})) = 0, \qquad \mathbf{x} \text{ on } \omega^* \tag{4.2}$$

with boundary values $w_i = f_i \in H^{1/2}(\partial\omega_I^*)$ and $w_i = 0$ on $\partial\omega_b^*$. These functions form a basis for an N-dimensional subspace of $\mathcal{A}_d(\omega^*)$. We denote this subspace by $W_d^N = \operatorname{span}\{w_1, w_2 \ldots, w_N\}$.

Working as before we construct finite dimensional subspaces of $\mathcal{A}_n(\omega^*)$ and $\mathcal{A}_d(\omega^*)$ with optimal approximation properties on ω adjacent to the boundary. For ease of exposition we will denote either $\mathcal{A}_n(\omega^*)$ and $\mathcal{A}_d(\omega^*)$ as $\mathcal{A}_B(\omega^*)$ and similarly $\mathcal{A}_n(\omega)$ and $\mathcal{A}_d(\omega)$ are denoted as $\mathcal{A}_B(\omega)$. The corresponding finite dimensional subspaces W_n^N and W_d^N are written as W_B^N. Now consider the restriction of functions in $\mathcal{A}_B(\omega^*)$ to ω. The restriction operator $R : \mathcal{A}_B(\omega^*) \to \mathcal{A}_B(\omega)$ is a compact operator [12]. The eigenvalues λ_j^B of R^*R decrease monotonically to zero with the index $j \to \infty$. We define $\{e_j\}_{j=1}^{\infty} \subset \mathcal{A}_B(\omega^*)$ to be the associated eigenfunctions given by

$$R^*Re_j = \lambda_j^B e_j,$$

or

$$(e_j, v)_{\mathcal{E}(\omega)} = \lambda_j^B (e_j, v)_{\mathcal{E}(\omega*)}, \tag{4.3}$$

for all $v \in \mathcal{A}_B(\omega^*)$. Here we take the normalization $(e_i, e_j)_{\mathcal{E}(\omega^*)} = \delta_{ij}$. The eigenvalues $\{\lambda_n^B\}_{n=1}^{\infty}$ form a decreasing sequence of positive real numbers and we order the eigenvalues according to max–min. The space spanned by M eigenfunctions corresponding to the eigenvalues $\{\lambda_n^B\}_{n=1}^{M}$ has optimal approximation properties. Denoting the optimal space by V_B^M this is expressed in the following theorem [10,12].

Theorem 4.1 (*Optimal Approximation Property*). *Given* $V_B^M = \operatorname{span}\{e_1, \ldots, e_M\}$ *and consider any* M *dimensional subspace* $W_B^M \subset \mathcal{A}(\omega^*)$ *then*

$$\sqrt{\lambda_{M+1}^B} = \sup_{u \in \mathcal{A}_B(\omega^*)} \inf_{e \in V_B^M} \frac{\|u - e\|_{\mathcal{E}(\omega)}}{\|u\|_{\mathcal{E}(\omega^*)}} = \inf_{W_B^M \subset \mathcal{A}_B(\omega^*)} \sup_{u \in \mathcal{A}_B(\omega^*)} \inf_{v \in W_B^M} \frac{\|u - v\|_{\mathcal{E}(\omega)}}{\|u\|_{\mathcal{E}(\omega^*)}}. \tag{4.4}$$

The best relative approximation error of a function $u \in \mathcal{A}_B(\omega^*)$ over ω by an element of a subspace $W_B^N \subset \mathcal{A}(\omega^*)$ of dimension M is given by the Sup-Inf,

$$\sqrt{\mu_N^B} = \sup_{u \in \mathcal{A}_B(\omega^*)} \inf_{v \in W_B^N} \frac{\|u - v\|_{\mathcal{E}(\omega)}}{\|u\|_{\mathcal{E}(\omega^*)}}. \tag{4.5}$$

A spectral characterization for the Sup-Inf that holds for partition of unity domains ω interior to Ω as well as on the boundary is given in Section 5. The spectral characterization provides a means for computing the Sup-Inf numerically. It is now evident that arguments of Section 3 can be applied immediately to domains adjacent to the boundary to deliver the analogous Theorems and Corollaries provided in Section 3 on applying the substitutions λ_i^B, μ_i^B, W_B^N and V_B^M in place of λ_i, μ_i, W^N and V^M.

5. Spectral definition of Sup-Inf

The Sup-Inf of the finite dimensional approximation space W^N is reformulated as a spectral problem. This formulation allows for the numerical computation of a-priori error estimates for the approximation of $u \in \mathcal{A}(\omega^*)$ or $u \in \mathcal{A}_B(\omega^*)$, by elements in a finite dimensional approximation space of $\mathbb{A}$-harmonic functions. The method for spectral definition Sup-Inf for the case of interior domains ω or domains adjacent to the boundary is the same. So without loss of generality we state the spectral representation in the context of interior domains $u \in \mathcal{A}(\omega^*)$. The restriction operator is explicitly written in terms of a prescribed Hilbert space basis of $\mathcal{A}(\omega^*)$ denoted by $\{w_i\}_{i=1}^{\infty}$. We shall take the basis to be orthonormal i.e., $(w_i, w_j)_{\mathcal{E}(\omega^*)} = \delta_{ij}$. Given $h \in \mathcal{A}(\omega^*)$ we have $h = \sum_{i=1}^{\infty}(w_i, h)_{\mathcal{E}(\omega^*)} w_i$, so the restriction operator $Rh = h|_\omega$ is given by

$$Rh = \sum_{i=1}^{\infty}(w_i, h)_{\mathcal{E}(\omega^*)} Rw_i, \qquad Rw_i = w_i|_\omega. \tag{5.1}$$

A straight forward computation shows that the adjoint of the restriction operator is

$$R^*h = \sum_{i=1}^{\infty}(w_i, h)_{\mathcal{E}(\omega)} w_i. \tag{5.2}$$

Set $RW^N = \text{span}\{Rw_1 \ldots, Rw_N\}$ and we preserve dimension under the restriction.

Theorem 5.1. *The dimension of the restriction of the space W^N to ω given by RW^N is N.*

Proof. Suppose instead there exist numbers $\{\alpha_i\}_{i=1}^N$ not all zero such that $\sum_i^N \alpha_i Rw_i = 0$ then $\sum_i^N \alpha_i w_i = 0$ on ω. Since $\sum_i^N \alpha_i w_i \in \mathcal{A}(\omega^*)$ we see from the unique continuation property [46,47] that $\sum_i^N \alpha_i w_i = 0$ in ω^*. Hence the dimension of W^N is less than N and we get the desired contradiction. □

Consider the projection $\mathbb{P}_{RW^N} : \mathcal{A}(\omega) \to RW^N$. This projection acting on Ru is written as $\mathbb{P}_{RW^N} Ru = \sum_{i=1}^N (Ru, Rw_i)_{\mathcal{E}(\omega)} Rw_i$ and $\mathbb{P}^*_{RW^N} u = \sum_{i=1}^N (u, R^*w_i)_{\mathcal{E}(\omega^*)} R^*w_i$. Denote the identity over $\mathcal{A}(\omega)$ by I_ω and set $Tu = (I_\omega - \mathbb{P}_{RW^N})Ru$. With this definition of T together with (3.5) we immediately have

$$\mu_N = \sup_{u\in\mathcal{A}(\omega^*)} \inf_{v\in W^N} \frac{\|u - v\|^2_{\mathcal{E}(\omega)}}{\|u\|^2_{\mathcal{E}(\omega^*)}} = \sup_{u\in\mathcal{A}(\omega^*)} \frac{(T^*Tu, u)_{\mathcal{E}(\omega^*)}}{\|u\|^2_{\mathcal{E}(\omega^*)}}. \tag{5.3}$$

Now we obtain the spectral representation of the Sup-Inf. Since $I_\omega - \mathbb{P}_{RW^N}$ is a bounded operator on $\mathcal{A}(\omega)$ there exists a positive constant C independent of u for which

$$\|Tu\|_{\mathcal{E}(\omega)} \le C\|Ru\|_{\mathcal{E}(\omega)}. \tag{5.4}$$

Since $R : \mathcal{A}(\omega^*) \to \mathcal{A}(\omega)$ is a compact operator it now follows that $T : \mathcal{A}(\omega^*) \to \mathcal{A}(\omega)$ is a compact operator. Collecting results we see that T^*T is a bounded, self-adjoint, compact operator on $\mathcal{A}(\omega^*)$ characterized by a countable nonincreasing sequence of positive eigenvalues $\nu_1^N \ge \nu_2^N \ge \cdots \searrow 0$. The eigenvalue problem for T^*T is given by the pairs $u \in \mathcal{A}(\omega^*)$, $\nu \in \mathbb{R}^+$ such that

$$((I_\omega - \mathbb{P}_{RW^N})Ru,\ (I_\omega - \mathbb{P}_{RW^N})Rv)_{\mathcal{E}(\omega)} = \nu(u, v)_{\mathcal{E}(\omega^*)} \qquad \text{for all } v \in \mathcal{A}(\omega^*). \tag{5.5}$$

The largest eigenvalue for this problem is ν_1^N and it is the Sup-Inf and denoted by μ_N. It is clear that μ_N is nonincreasing with N. This formula is used to compute the Sup-Inf in the numerical examples.

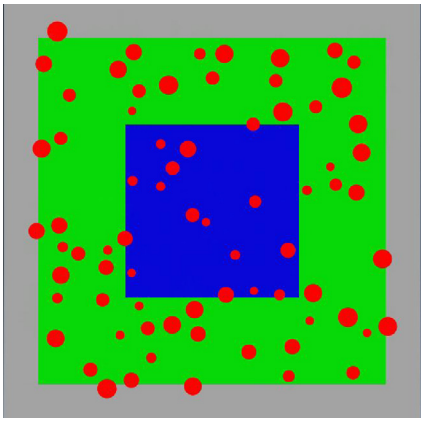

Fig. 3. A microgeometry similar to [13], Fig. 2. The side length of ω^* domain to side length of ω is of ratio 2 : 1.

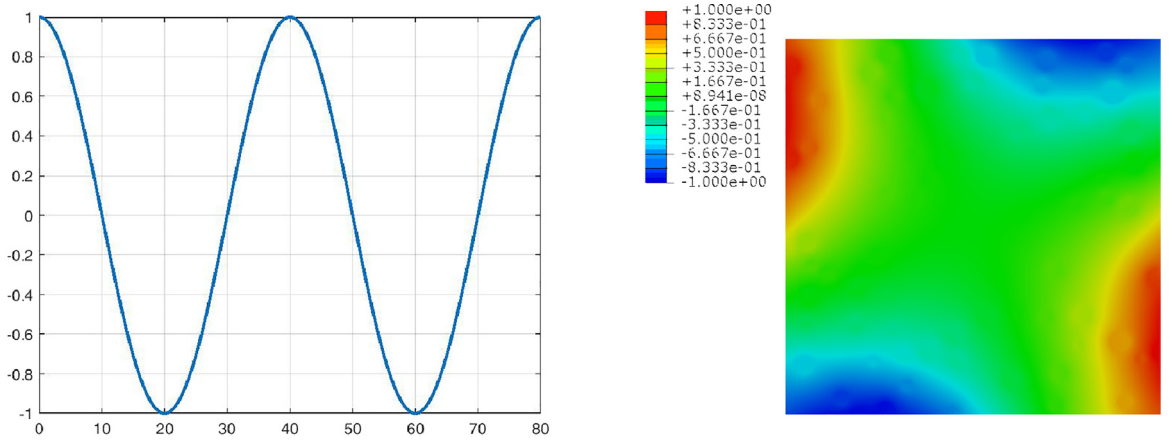

Fig. 4. Applied Dirichlet boundary conditions (left) and resulting $\mathbb{A}$-harmonic extension (right) for g_2^1.

6. The discrete problem

In this section we consider finite element discretizations of the local problem in two dimensions. We describe the case for ω in the interior of Ω, as in Fig. 3. Here the blue square represents ω, the union of blue and green domains represents ω^* and the union of blue, green and, gray domains represents Ω. Here $\mathbb{A}$ is associated with the coefficient of a particulate composite taking on one constant value in the particles (in red) and another outside. Take a triangular partition of ω^* of size h and choose a set of L functions from a countable set of functions that form a basis in $L^2(\partial\omega^*)$ consistent with the triangulation of size h. The discrete $\mathbb{A}_L$-harmonic extension of the boundary data is given in terms of a bi-linear finite element (FE) basis. The size of the FE mesh h is consistent with the smallest length scale of the boundary oscillations. For example if we choose $\mathbb{A}$-harmonic extensions of the boundary values $\sin(kt)$, $\cos(kt)$ for $k = 1, \ldots, L/2$ and t parameterizes the boundary, then it is found that, for a given minimum particle diameter d and contrast between material properties, a consistent choice of the length scale h of the FE mesh in ω^* is $h \approx \min\{\frac{d}{10}, \frac{1}{10L}\}$. We apply Gram–Schmidt to the system of linearly independent $\mathbb{A}$-harmonic extensions of the L boundary basis functions to recover an orthonormal basis $\{w_j\}_{j=1}^L$ with respect to the energy inner product on ω^*. Fig. 4 shows the $\mathbb{A}$-harmonic extension of boundary data $\cos(2t)$ restricted to ω and Fig. 5 shows the $\mathbb{A}$-harmonic extension of piecewise linear boundary data restricted to ω.

The span of $w_1, \ldots, w_L$ is denoted by $\mathcal{A}_L(\omega^*)$. The restriction of functions in $\mathcal{A}_L(\omega^*)$ to ω is denoted by R. The eigenvalues λ_j of R^*R decrease monotonically as the index $j \to L$. We define $\{e_j\}_{j=1}^L \subset \mathcal{A}_L(\omega^*)$ to be the

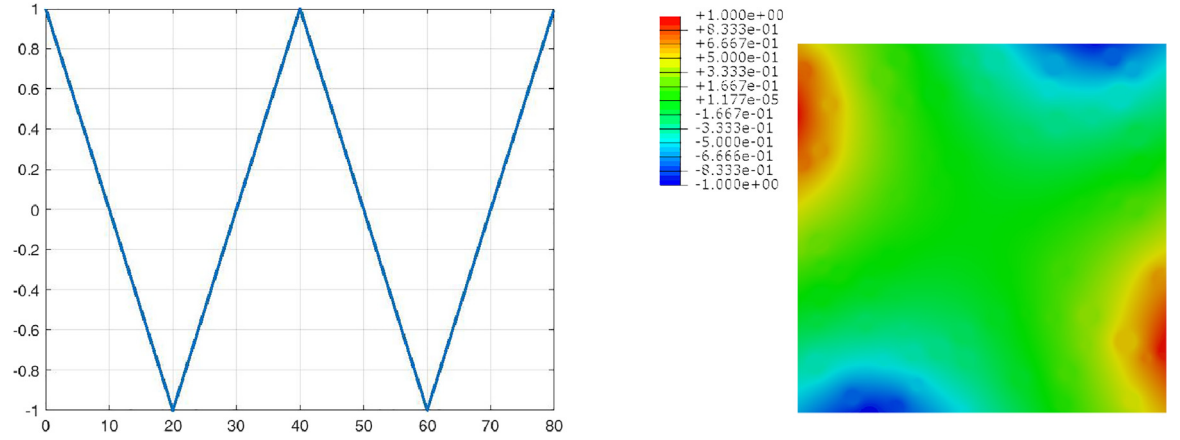

Fig. 5. Applied Dirichlet boundary conditions (left) and resulting $\mathbb{A}$-harmonic extension (right) for h_2^1.

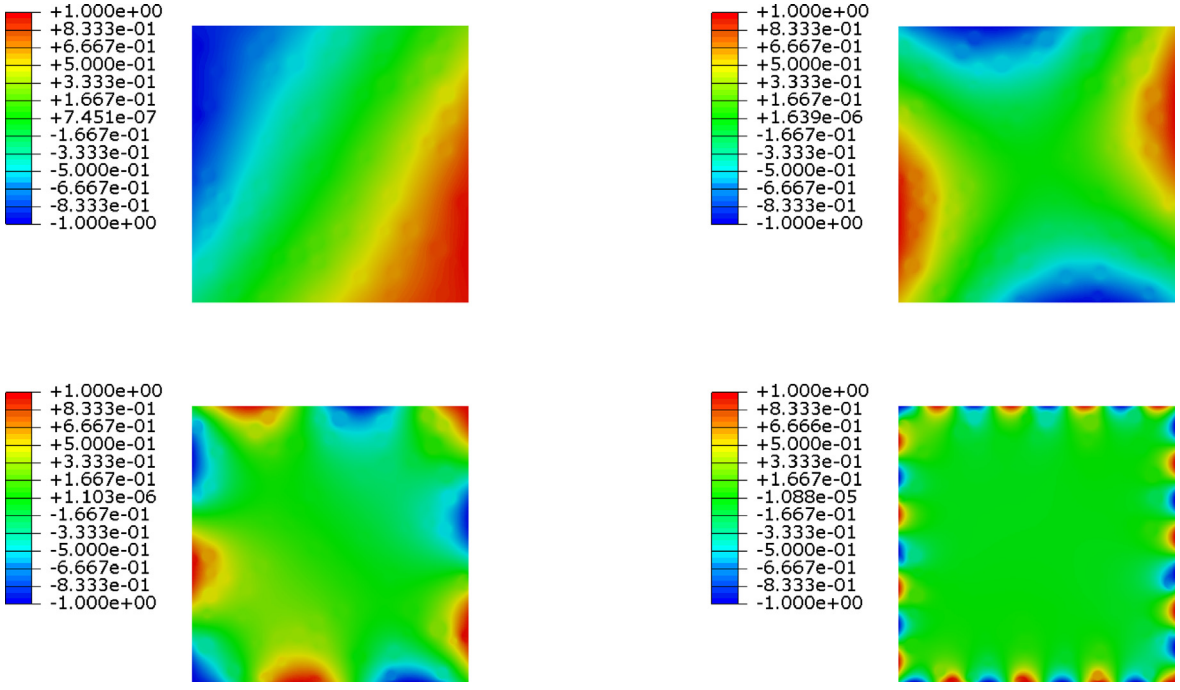

Fig. 6. $\mathbb{A}$-harmonic functions over ω^* created with boundary data ((7.1) left) for $n_1 = 1, n_1 = 5$ (left) and ((7.1) right) for $n_2 = 2, n_2 = 15$ (right).

associated eigenfunctions given by

$$R^* R e_j = \lambda_j e_j, \tag{6.1}$$

or

$$(e_j, v)_{\mathcal{E}(\omega)} = \lambda_j (e_j, v)_{\mathcal{E}(\omega*)}, \tag{6.2}$$

for all $v \in \mathcal{A}_L(\omega^*)$. Here we take the normalization $(e_i, e_j)_{\mathcal{E}(\omega^*)} = \delta_{ij}$. As before we have,

Theorem 6.1. *Given* $V^M = \text{span}\{e_1, \ldots, e_M\}$ *and consider any* M *dimensional subspace* $W^M \subset \mathcal{A}_L(\omega^*)$ *then*

$$\sqrt{\lambda_{M+1}} = \sup_{u \in \mathcal{A}_L(\omega^*)} \inf_{e \in V^M} \frac{\|u - e\|_{\mathcal{E}(\omega)}}{\|u\|_{\mathcal{E}(\omega^*)}} = \inf_{W^M \subset \mathcal{A}_L(\omega^*)} \sup_{u \in \mathcal{A}_L(\omega^*)} \inf_{v \in W^M} \frac{\|u - v\|_{\mathcal{E}(\omega)}}{\|u\|_{\mathcal{E}(\omega^*)}}. \tag{6.3}$$

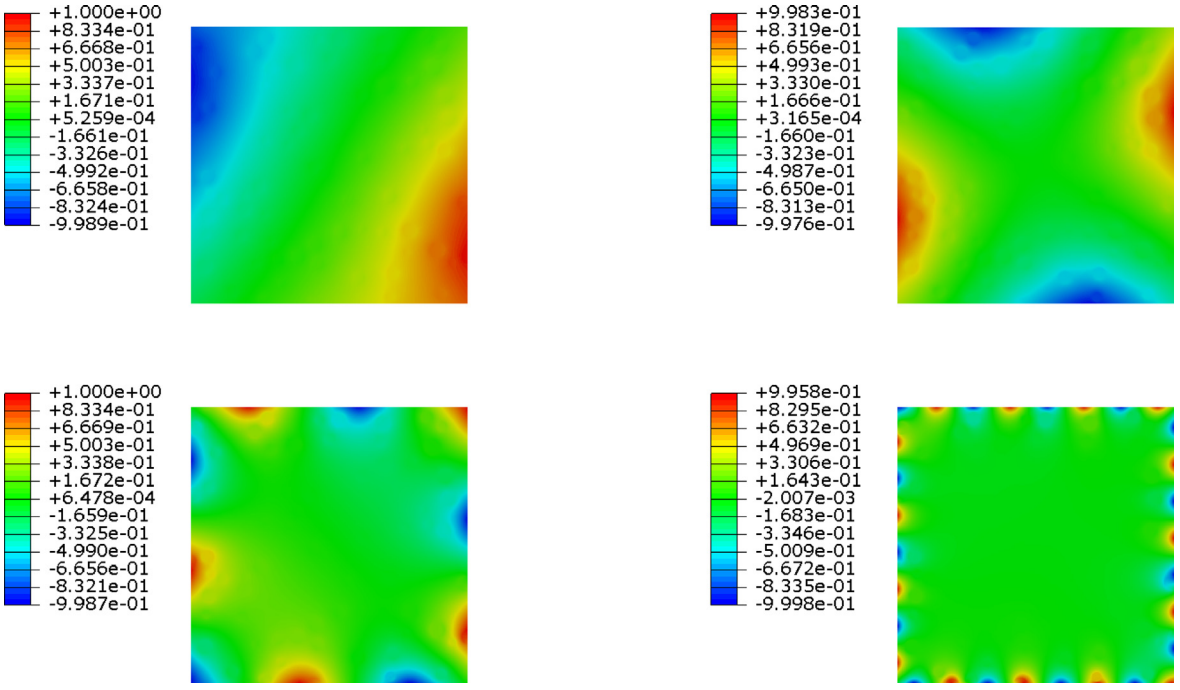

Fig. 7. $\mathbb{A}$-harmonic functions over ω^* created with boundary data ((7.2) left) for $n_1 = 1, n_1 = 5$ (left) and ((7.2) right) for $n_2 = 2, n_2 = 15$ (right).

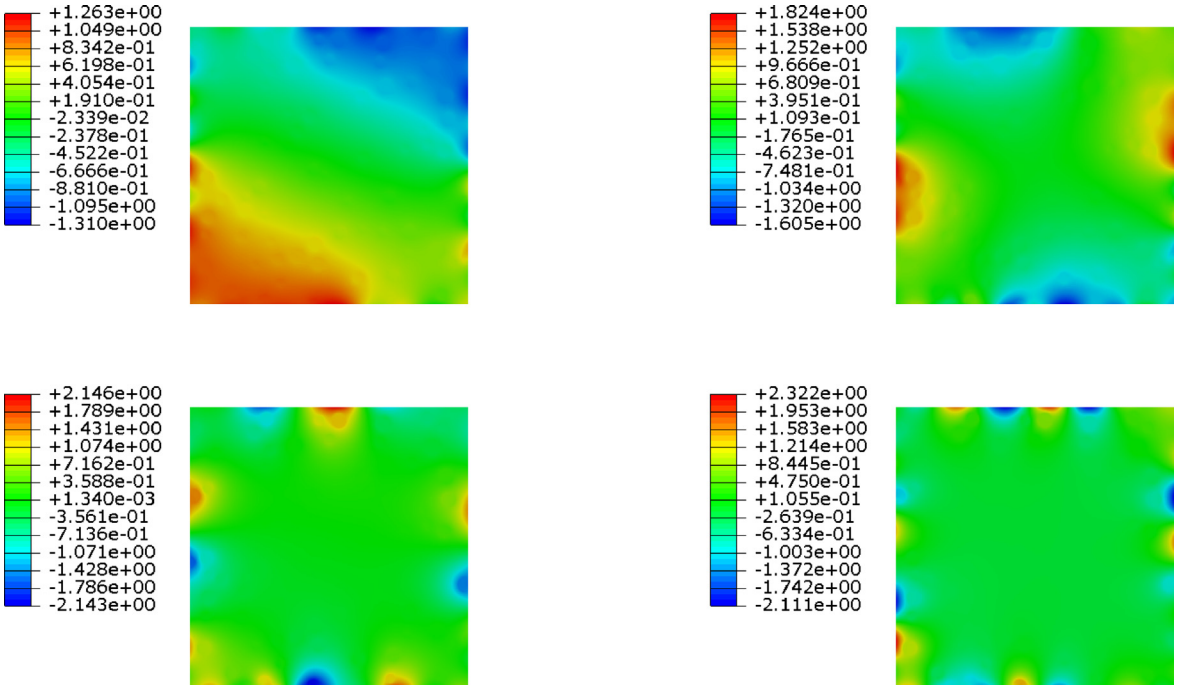

Fig. 8. Eigenfunctions in ω^* for eigenvalues $\lambda_1, \lambda_4, \lambda_9, \lambda_{16}$.

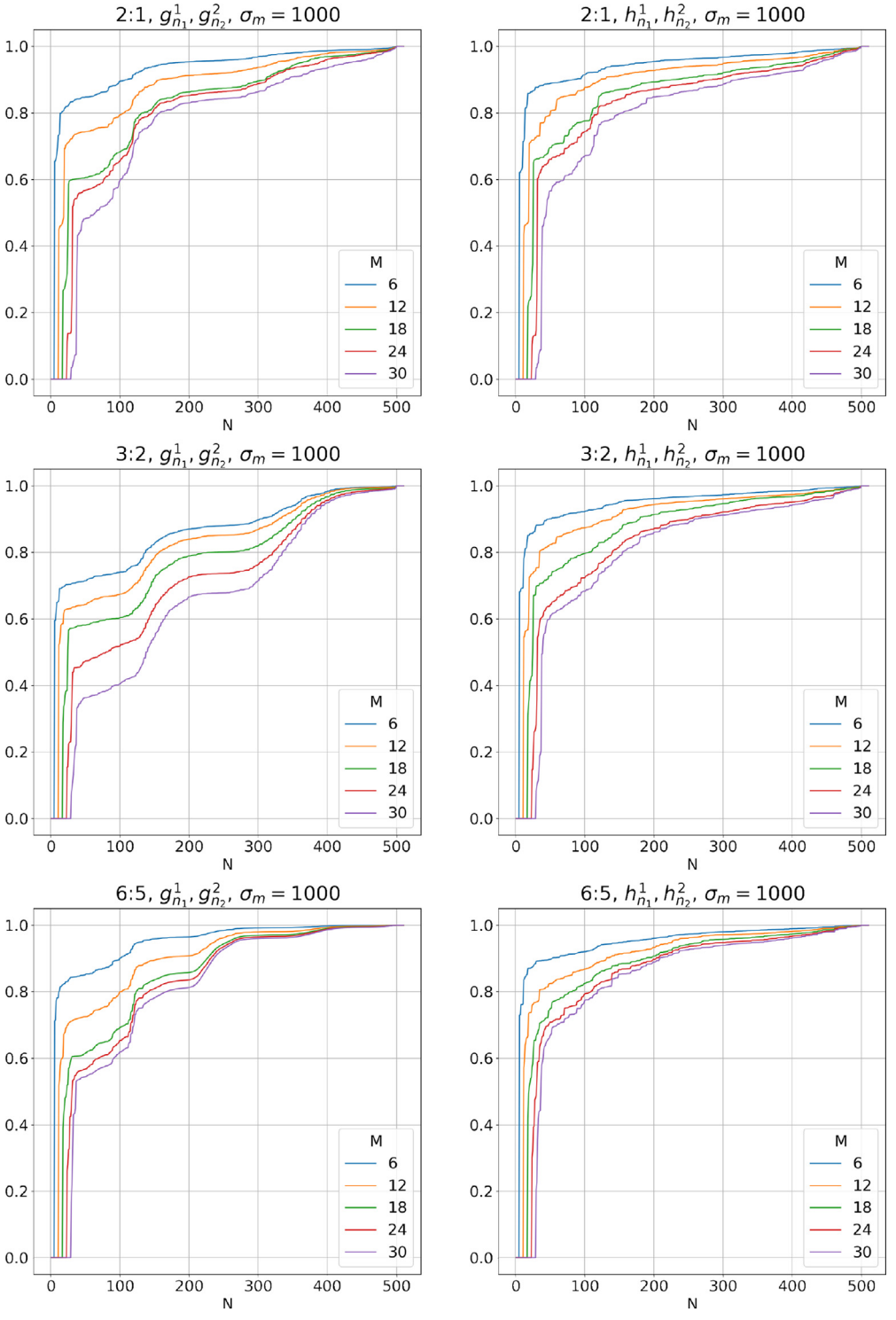

Fig. 9. Cosine computations for $\sigma_m = 1000$ with a mesh of 10 million elements on ω^*. The cosine is computed between a fixed number M of eigenfunctions of the restriction operator (each line in the plots) and the space of $\mathbb{A}$-harmonic functions. In the left column the $\mathbb{A}$-harmonics are $g^1_{n_1}$, $g^2_{n_2}$, and in the right column $h^1_{n_1}$, $h^2_{n_2}$. The eigenfunctions are computed using the same boundary data as used to generate the $\mathbb{A}$-harmonic functions.

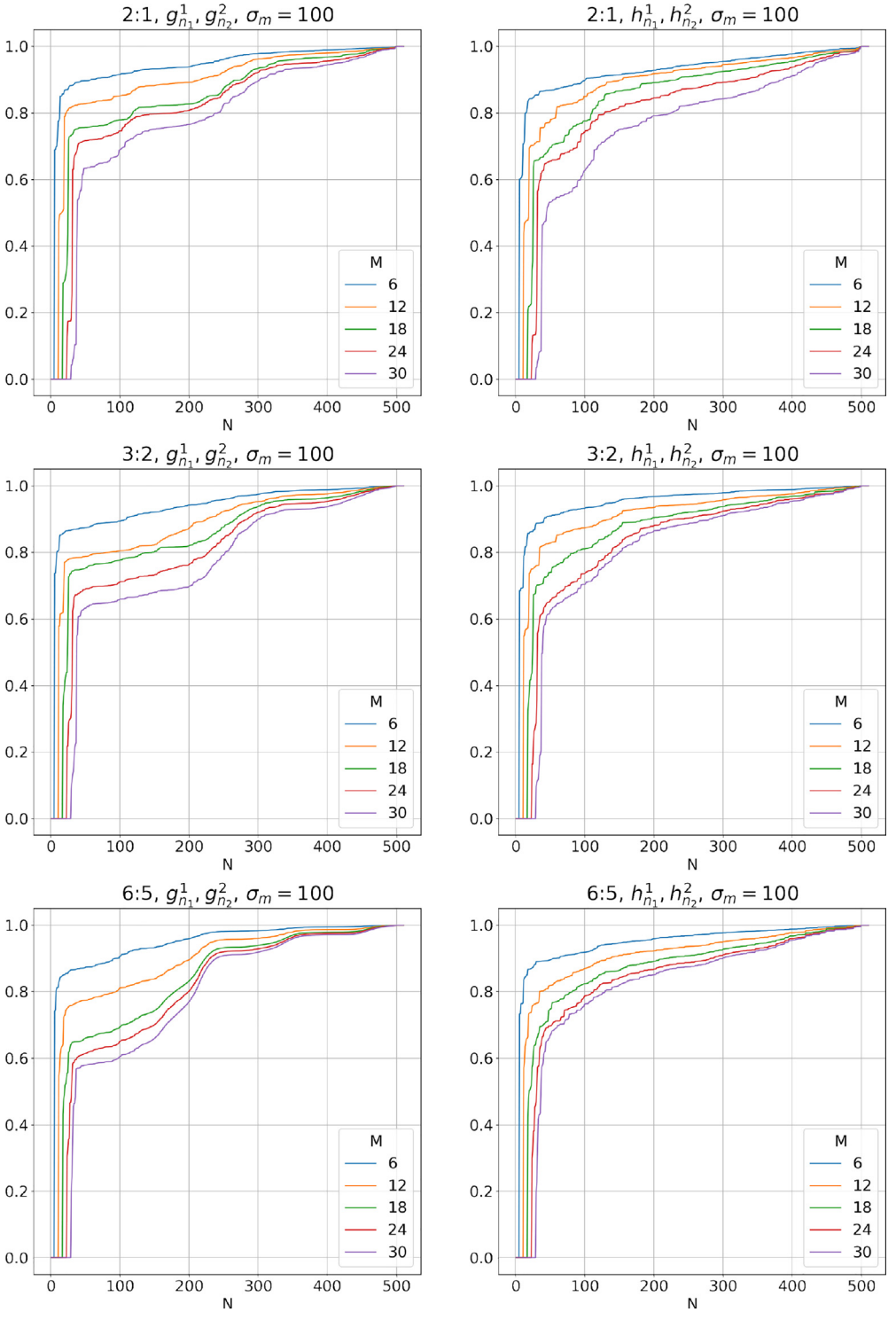

Fig. 10. Cosine computations for $\sigma_m = 100$ with a mesh of 10 million elements on ω^*. The cosine is computed between a fixed number M of eigenfunctions of the restriction operator (each line in the plots) and the space of $\mathbb{A}$-harmonic functions. In the left column the $\mathbb{A}$-harmonics are $g^1_{n_1}$, $g^2_{n_2}$, and in the right column $h^1_{n_1}$, $h^2_{n_2}$. The eigenfunctions are computed using the same boundary data as used to generate the $\mathbb{A}$-harmonic functions.

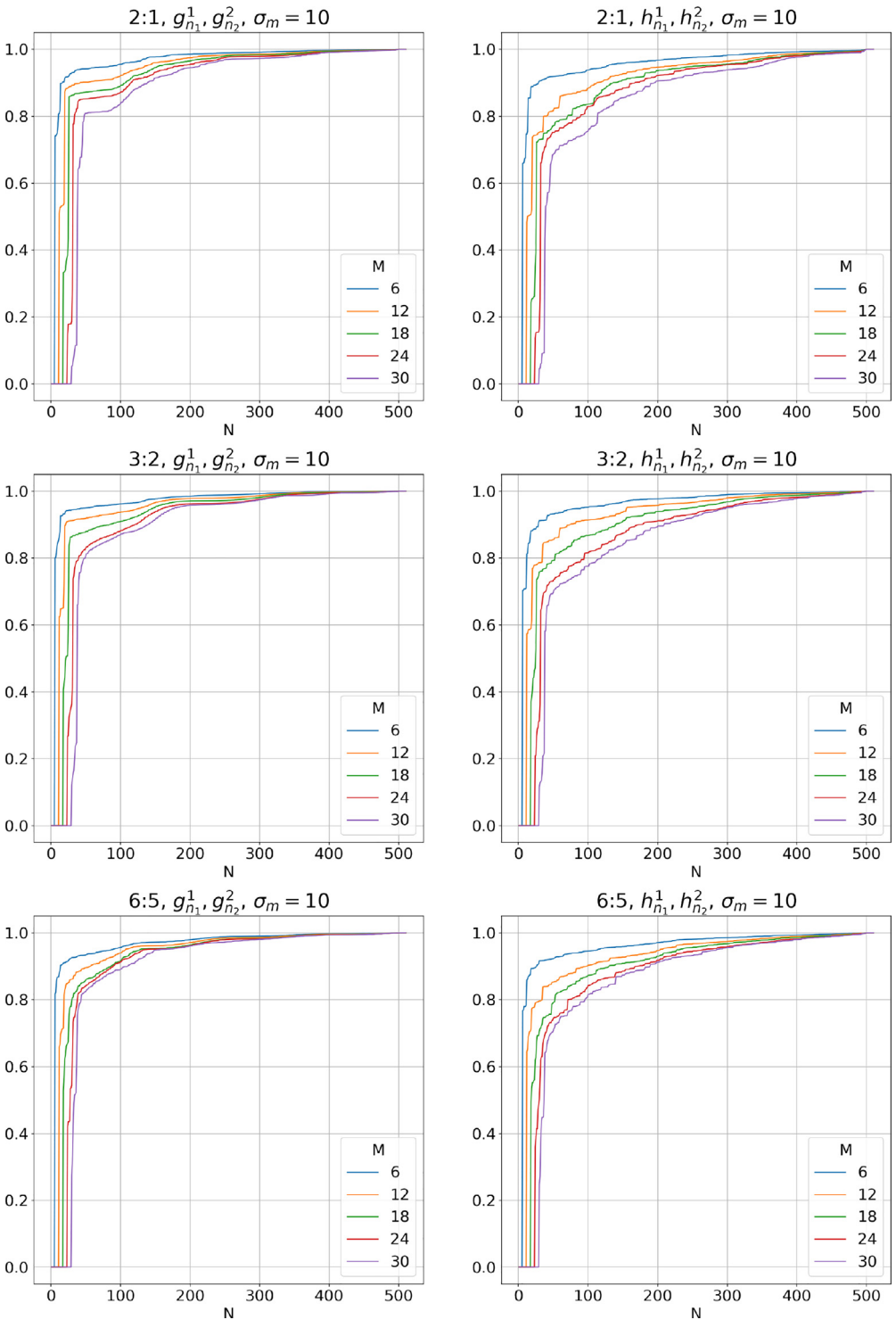

Fig. 11. Cosine computations for $\sigma_m = 10$ with a mesh of 10 million elements on ω^*. The cosine is computed between a fixed number M of eigenfunctions of the restriction operator (each line in the plots) and the space of $\mathbb{A}$-harmonic functions. In the left column the $\mathbb{A}$-harmonics are $g^1_{n_1}$, $g^2_{n_2}$, and in the right column $h^1_{n_1}$, $h^2_{n_2}$. The eigenfunctions are computed using the same boundary data as used to generate the $\mathbb{A}$-harmonic functions.

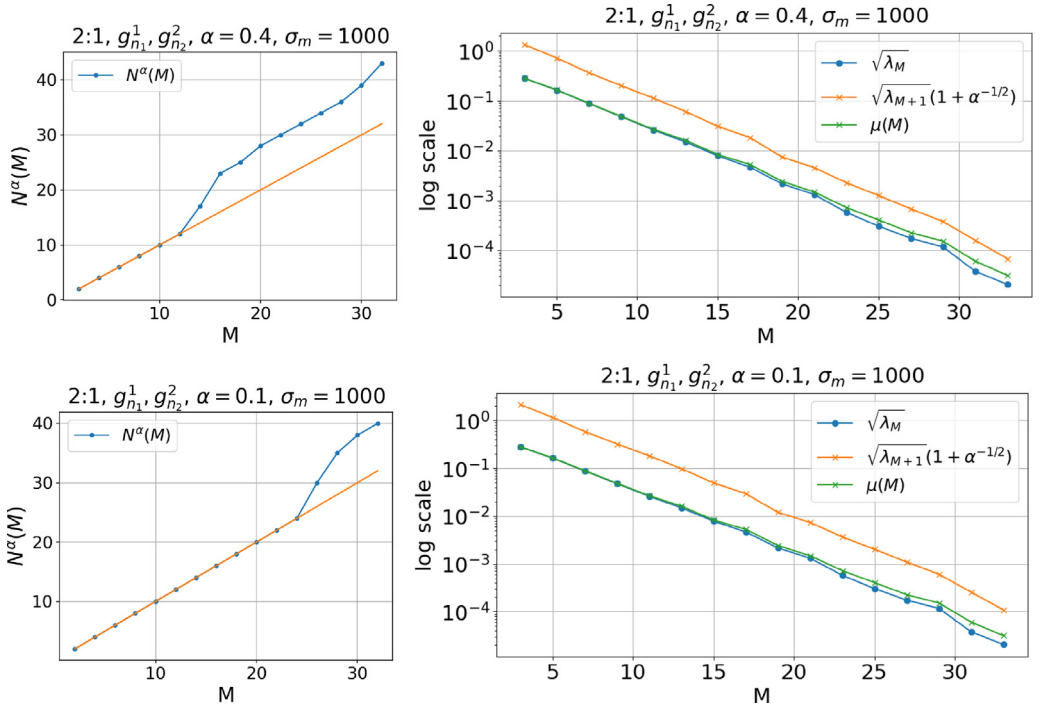

Fig. 12. The left column shows plots of $N^\alpha(M)$ in blue compared to the identity line in orange. The right column shows $\mu(M)$ compared to the eigenvalues of the restriction operator and the bound of Theorem 3.8. All plots are on a domain with oversampling ratio of 2:1 and conductivity $\sigma_m = 1000$ in the connected phase. The space $\mathcal{A}(\omega^*)$ is generated by cosines and sines as boundary data. The top row has $\alpha = 0.4$ and the bottom row has $\alpha = 0.1$. (For interpretation of the references to color in this figure legend, the reader is referred to the web version of this article.)

The relative approximation error of $\mathcal{A}_L(\omega)$ functions by an element of $W^N \subset \mathcal{A}_L(\omega^*)$ is given by the Sup-Inf,

$$\mu(N) = \sup_{u \in \mathcal{A}_L(\omega^*)} \inf_{v \in W^N} \frac{\|u - v\|_{\mathcal{E}(\omega)}}{\|u\|_{\mathcal{E}(\omega^*)}}. \tag{6.4}$$

As before it is now evident that arguments of Section 3 can be applied immediately to deliver the analogous Theorems and Corollaries provided in Section 3.

7. Numerical simulations

The domains $\omega \subset \omega^*$ within the composite domain are given by nested rectangles as in Fig. 3. Here ω is the blue region and ω^* is the union of the blue region and the green picture frame. The ratio of side lengths of the outer and inner rectangles are two to one. We call this an oversampling ratio of $2:1$. The composite is composed of particles embedded within a connected phase. Here $\mathbb{A} = \mathbb{I}$ inside the particles and $\mathbb{A} = \sigma_m \mathbb{I}$ in the connected phase.

In a first example we generate $\mathbb{A}$-harmonic functions using sines and cosines as Dirichlet boundary conditions. *We order the boundary data according to increasing frequency of oscillation* generating a 500-dimensional space. To apply these functions, the boundary $\partial\omega^*$ of length L is parameterized. The parameter t starts at a given node on the boundary and runs along it until it hits the node again. The 500 sines and cosines are given by the following, for $n_1 = 1, \ldots, 250$ and $n_2 = 1, \ldots, 250$,

$$g^1_{n_1}(t) = \cos\left(\frac{2\pi n_1 t}{L}\right), \quad g^2_{n_2}(t) = \sin\left(\frac{2\pi n_2 t}{L}\right). \tag{7.1}$$

The $\mathbb{A}$-harmonic extension of $g^1_2(t)$ over ω^* is given in Fig. 4. Examples of $\mathbb{A}$-harmonic extensions for different $g^1_{n_1}$ and $g^2_{n_2}$ are given in Fig. 6. Eigenfunctions that participate in the optimal approximation space associated with

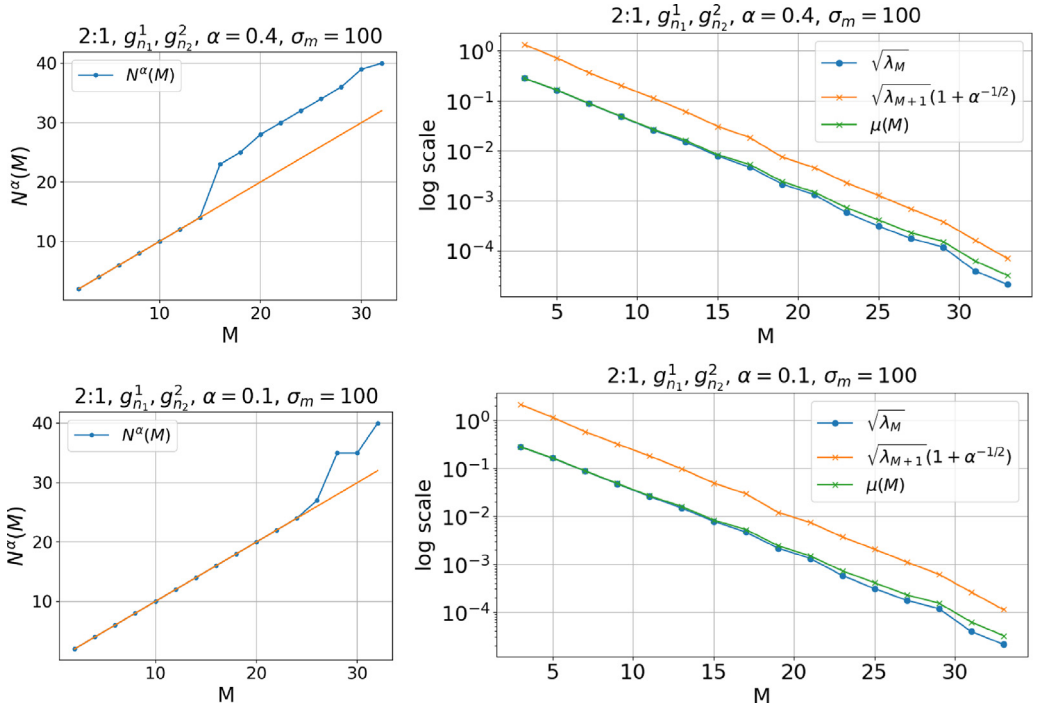

Fig. 13. The left column shows plots of $N^\alpha(M)$ in blue compared to the identity line in orange. The right column shows $\mu(M)$ compared to the eigenvalues of the restriction operator and the bound of Theorem 3.8. All plots are on a domain with oversampling ratio of 2:1 and conductivity $\sigma_m = 100$ in the connected phase. The space $\mathcal{A}(\omega^*)$ is generated by cosines and sines as boundary data. The top row has $\alpha = 0.4$ and the bottom row has $\alpha = 0.1$. (For interpretation of the references to color in this figure legend, the reader is referred to the web version of this article.)

$\lambda_1, \lambda_4, \lambda_9, \lambda_{16}$ inside ω are given in Fig. 8. In a second example we use piecewise linear functions which are parameterized on the boundary as

$$h^1_{n_1}(t) = C\left(t \mod \frac{L}{n}\right), \quad h^2_{n_2}(t) = S\left(t \mod \frac{L}{n}\right) \tag{7.2}$$

for

$$C(x) = \begin{cases} -4(x - \frac{1}{4}) & x \in [0, \frac{1}{2}] \\ 4(x - \frac{3}{4}) & x \in [\frac{1}{2}, 1], \end{cases} \quad S(x) = \begin{cases} 4x & x \in [0, \frac{1}{4}] \\ -4(x - \frac{1}{2}) & x \in [\frac{1}{4}, \frac{3}{4}] \\ 4(x - \frac{3}{4}) & x \in [\frac{3}{4}, 1]. \end{cases} \tag{7.3}$$

Again the bases are indexed in order of increasing frequency of oscillation Note that $h^1_{n_1}(t)$ and $h^2_{n_2}(t)$ are piecewise linear approximations of $g^1_{n_1}(t)$ and $g^2_{n_2}(t)$, respectively. The $\mathbb{A}$-harmonic extension of $h^1_2(t)$ over ω^* is given in Fig. 5. Examples of $\mathbb{A}$-harmonic extensions for different $h^1_{n_1}$ and $h^2_{n_2}$ are given in Figs. 7 and 8 shows the optimal basis functions given by the eigenfunctions of the restriction operator. They are computed using the $\mathbb{A}$-harmonic extensions generated by cosines and sines (7.1). The eigenfunctions with eigenvalues $\lambda_1, \lambda_4, \lambda_9, \lambda_{16}$ oscillate on the boundary at the same frequency as g^1_1, g^2_2, g^1_5, and g^2_8. Figs. 6 through 8 show that the $\mathbb{A}$-harmonic extensions of boundary given by trigonometric boundary data $g^1_{n_1}$, $g^2_{n_2}$ or oscillatory linear boundary data $h^1_{n_1}$, $h^2_{n_2}$ oscillate on the boundary to the same degree as the optimal basis functions given by the eigenfunctions of the restriction operator.

In Figs. 9 through 11 we examine the function $\sqrt{\alpha} = \cos\beta^N_M$ as it depends on the oversampling ratio, the choice of $\mathbb{A}$-harmonic extensions of boundary data, and σ_m. The outer square domain ω^* has side length denoted by L_{out}. The concentric inner square domain ω has side length L_{in}. The ratio of the side lengths is denoted by $L_{out} : L_{in}$. Each graph corresponds to a fixed choice of $L_{out} : L_{in}$, σ_m, and local basis generated by $g^1_{n_1}$, $g^2_{n_2}$ or $h^1_{n_1}$, $h^2_{n_2}$. Each graph portrays five curves of $\sqrt{\alpha} = \cos\beta^N_M$ for a different fixed value of M. The blue curve corresponds to $M = 6$,

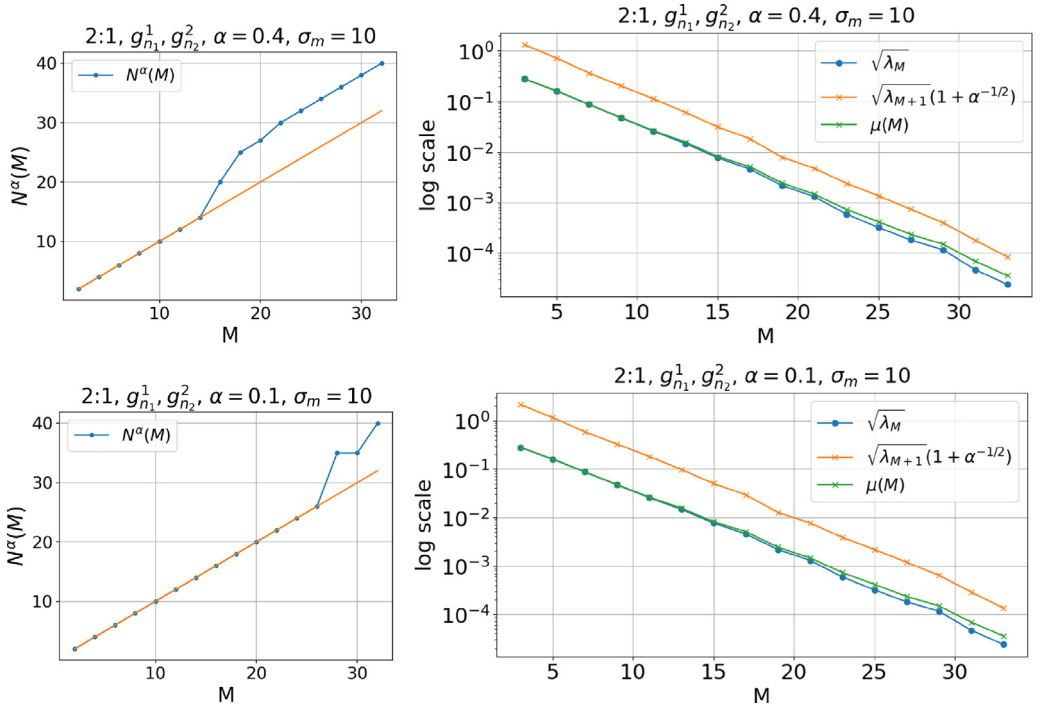

Fig. 14. The left column shows plots of $N^\alpha(M)$ in blue compared to the identity line in orange. The right column shows $\mu(M)$ compared to the eigenvalues of the restriction operator and the bound of Theorem 3.8. All plots are on a domain with oversampling ratio of 2:1 and conductivity $\sigma_m = 10$ in the connected phase. The space $\mathcal{A}(\omega^*)$ is generated by cosines and sines as boundary data. The top row has $\alpha = 0.4$ and the bottom row has $\alpha = 0.1$. (For interpretation of the references to color in this figure legend, the reader is referred to the web version of this article.)

the red curve corresponds to $M = 12$, the green curve corresponds to $M = 18$, the orange curve corresponds to $M = 24$, and the purple curve corresponds to $M = 30$. For all plots N runs from 1 to 500 and $\alpha \in [0, 1]$. Here $\alpha = 0$ for $N < M$ and $\alpha = 1$ for $N \geq 500$. In all cases $\alpha > 0$ when $N = M + 2$, however as M is increased the growth rate of α with N decreases and the growth rate of all curves decrease with increasing σ_m. The growth rate of α with N remains roughly the same for all curves as the oversampling $L_{out} : L_{in}$ runs from $2 : 1$ to $6 : 5$.

We now fix the oversampling ratio to $2 : 1$ and provide plots of $\sqrt{\lambda_M}$, $\sqrt{\mu_M}$ and the bound $\sqrt{\lambda_{M+1}}(1 + \alpha^{-1/2})$ with $\alpha = 0.4$ and $\alpha = 0.1$ for the three choices $\sigma_m = 1000$, $\sigma_m = 100$, and $\sigma_m = 10$. Here we use local basis functions generated by the $\mathbb{A}$-harmonic extensions of trigonometric boundary data $g^1_{n_1}$, $g^2_{n_2}$. These studies are given in Figs. 12, 13, and 14. The same study is repeated for the local basis functions generated by the $\mathbb{A}$-harmonic extensions of piecewise linear boundary data $h^1_{n_1}$, $h^2_{n_2}$ in Figs. 15, 16, and 17. These figures also include plots of $N^\alpha(M)$ for α fixed and M increasing with an identity line in orange for reference.

These studies show that the decay of $\sqrt{\lambda_M}$, $\sqrt{\mu_M}$, and $\sqrt{\lambda_{M+1}}(1 + \alpha^{-1/2})$ are all exponential in M. In all cases the curves $\sqrt{\lambda_M}$, $\sqrt{\mu_M}$ lie on top of each other for all choices of σ_m. The upper bound $\sqrt{\lambda_{M+1}}(1 + \alpha^{-1/2})$ is seen to lie well above the actual Sup-Inf values. These trends hold for the $\mathbb{A}$-harmonic extensions of $g^1_{n_1}$, $g^2_{n_2}$ and $h^1_{n_1}$, $h^2_{n_2}$. Figs. 12 through 17, show for all cases that $M \leq N^\alpha(M) \leq M + 10$. Additionally, we note that from $\alpha = 0.1$ to $\alpha = 0.4$, in each plot, the value of $N^\alpha(M)$ lifts off the identity line ($N^\alpha(M) > M$) for smaller M as α is increased. This trend holds as α is increased further. Since the optimal basis functions are seen to increase in oscillatory behavior along $\partial\omega^*$ as M increases, this indicates that an increasingly larger basis of $\mathbb{A}$-harmonic functions, $h^1_{n_1}$, $h^2_{n_2}$, $g^1_{n_1}$, and $g^2_{n_2}$, are required to sufficiently capture the higher order optimal basis functions.

8. Conclusion

We conclude from the numerical simulations that the subspaces both of $\mathbb{A}$-harmonic extensions of trigonometric functions and oscillatory linear functions deliver an exponentially decaying upper bound on the error. The

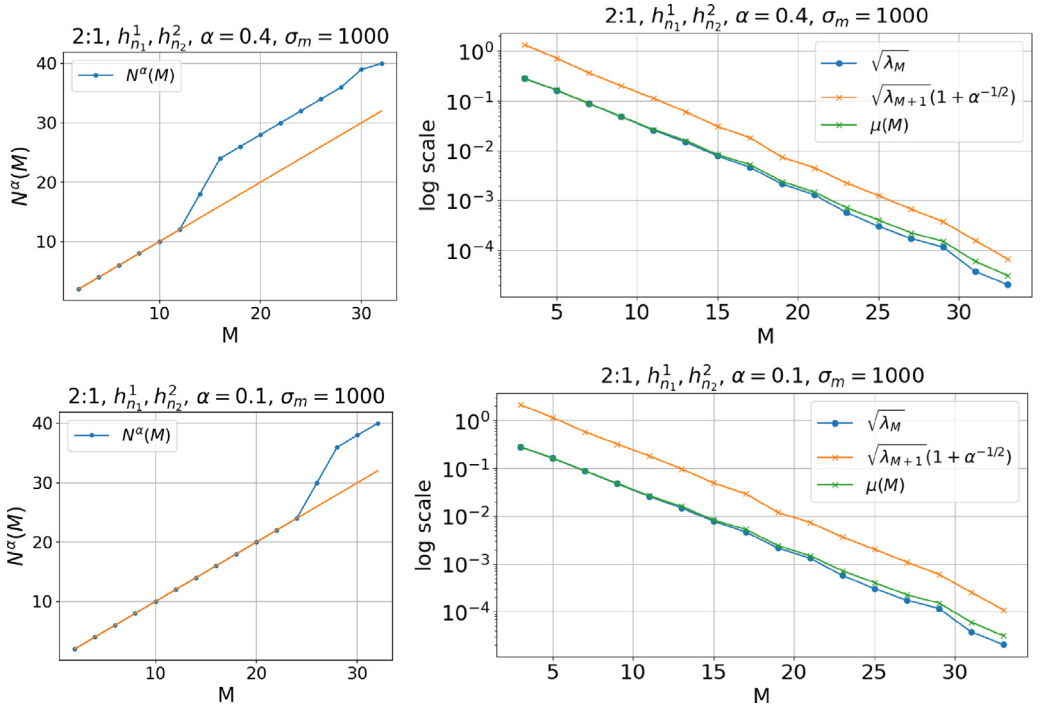

Fig. 15. The left column shows plots of $N^\alpha(M)$ in blue compared to the identity line in orange. The right column shows $\mu(M)$ compared to the eigenvalues of the restriction operator and the bound of Theorem 3.8. All plots are on a domain with oversampling ratio of 2:1 and conductivity $\sigma_m = 1000$ in the connected phase. The space $\mathcal{A}(\omega^*)$ is generated by piecewise linear functions as boundary data. The top row has $\alpha = 0.4$ and the bottom row has $\alpha = 0.1$. (For interpretation of the references to color in this figure legend, the reader is referred to the web version of this article.)

simulations show that the upper bound on convergence rate with respect to dimension for $W^{N^\alpha(M)}$ matches the actual decay of the optimal basis V^M with respect to M. For these cases $\beta^N_M \in (0, \pi/2]$ and $\alpha = \cos^2 \beta^N_M$ is taken to be 0.1 and 0.4 in the simulations. The bound corroborates the exponential convergence of the error between the basis and the actual solution seen in other simulations [9]. We point out that we use $\mathbb{A}$-harmonic basis functions that are extensions of complete bases of $H^{1/2}(\partial\omega^*)$ for interior domains ω^* and similarly for domains ω^* adjacent to the boundary $\partial\Omega$. We choose the boundary data be oscillatory with the same frequency of oscillation as the restriction of the optimal local basis to $\partial\omega^*$. The physical reason for this is that errors of highly oscillatory nature get damped out by the buffer domain $\omega^* \cap \omega^c$ and only lower oscillatory errors need to be eliminated over ω. This is in keeping with observations in [48] where this phenomenon is viewed from the perspective of energy concentration in ω. Oscillation enhanced decay away from the boundary is seen for the $\mathbb{A}$-harmonic extensions of trigonometric and oscillatory linear boundary data and the optimal basis, see Figs. 6 through 8. It is also seen in explicit computation of the eigenfunctions of R^*R for harmonic functions on the disk and sphere. Similar trends can be seen for the interior fields of $\mathbb{A}$-harmonic extensions harmonic polynomials [13] and Stekloff eigenfunctions in high contrast particulate media [49].

Declaration of competing interest

The authors declare that they have no known competing financial interests or personal relationships that could have appeared to influence the work reported in this paper.

Data availability

No data was used for the research described in the article.

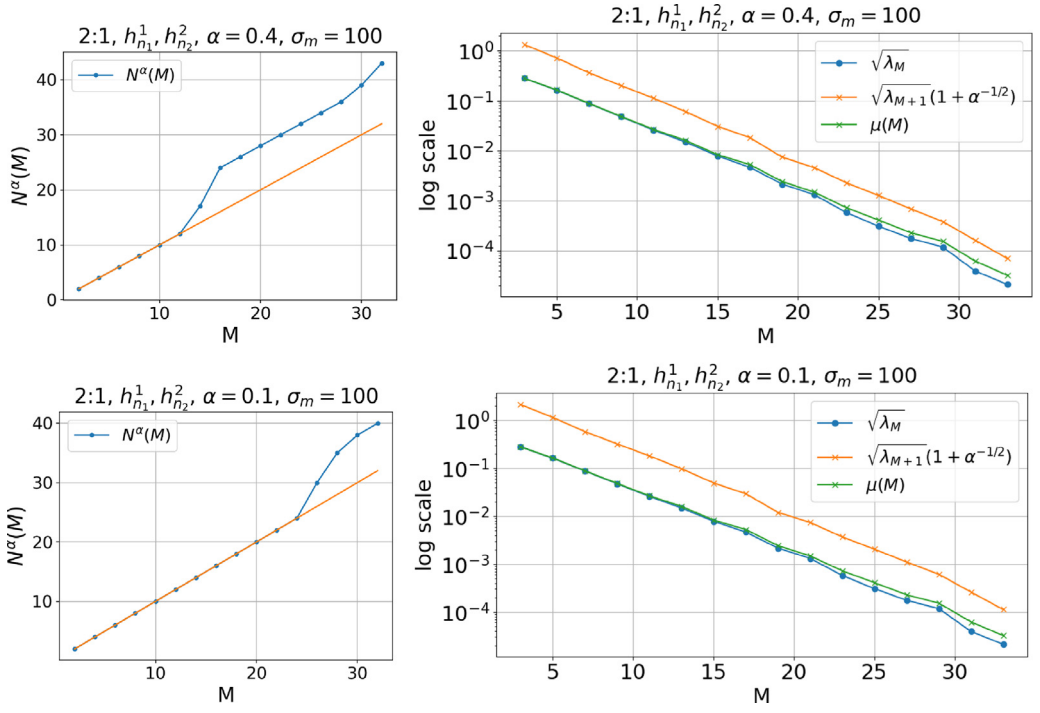

Fig. 16. The left column shows plots of $N^\alpha(M)$ in blue compared to the identity line in orange. The right column shows $\mu(M)$ compared to the eigenvalues of the restriction operator and the bound of Theorem 3.8. All plots are on a domain with oversampling ratio of 2:1 and conductivity $\sigma_m = 100$ in the connected phase. The space $\mathcal{A}(\omega^*)$ is generated by piecewise linear functions as boundary data. The top row has $\alpha = 0.4$ and the bottom row has $\alpha = 0.1$. (For interpretation of the references to color in this figure legend, the reader is referred to the web version of this article.)

Acknowledgments

The authors would like to thank Richard Tsai for pointing out that the angles introduced here are the Grassman angles between subspaces. This research work is supported in part by NSF, United States Grant DMS-1813698.

Appendix. Minimum eigenvalue is cosine

This appendix establishes the identity given by (3.7). Recall $A_{ij} = (e_i, w_j)_{\mathcal{E}(\omega^*)}$, and for $\vec{x} \in \mathbb{R}^M$ the minimum eigenvalue of the symmetric matrix AA^T is

$$\lambda_{MIN}(AA^T) = \min_{\vec{x}\in\mathbb{R}^M}\{\frac{AA^T\vec{x}\cdot\vec{x}}{|\vec{x}|^2}\}. \tag{A.1}$$

Define the subspaces $V^M = \text{span}\{e_1, \ldots, e_M\}$ as before and $W^N = \text{span}\{w_1, \ldots, w_N\}$, where $\{e_i\}_{i=1}^M$ and $\{w_i\}_{i=1}^N$ are orthonormal systems with respect to the inner product $(\cdot,\cdot)_{\mathcal{E}(\omega^*)}$. The orthogonal projection $\mathbb{P}_{W^N}$ of vectors e in $V^M = \text{span}\{e_1, \ldots, e_M\}$ into $W^N = \text{span}\{w_1, \ldots, w_N\}$ is defined by

$$\mathbb{P}_{W^N} e = \sum_{i=1}^{N} (w_i, e)_{\mathcal{E}(\omega^*)} w_i. \tag{A.2}$$

Now for $e = \sum_{i=1}^M x_i e_i$ note that $\|e\|^2_{\mathcal{E}(\omega^*)} = |\vec{x}|^2$. Then

$$\lambda_{MIN}(AA^T) = \tag{A.3}$$

$$= \min_{\vec{x}\in\mathbb{R}^M}\{\frac{AA^T\vec{x}\cdot\vec{x}}{\|e\|^2_{\mathcal{E}(\omega^*)}}\} \tag{A.4}$$

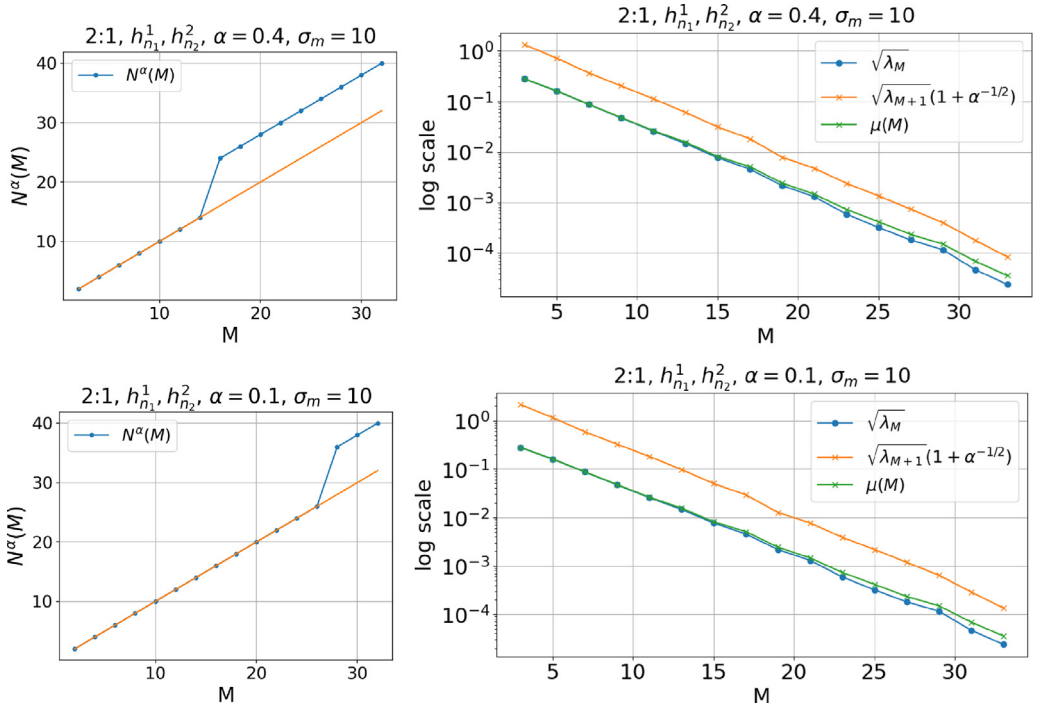

Fig. 17. The left column shows plots of $N^\alpha(M)$ in blue compared to the identity line in orange. The right column shows $\mu(M)$ compared to the eigenvalues of the restriction operator and the bound of Theorem 3.8. All plots are on a domain with oversampling ratio of 2:1 and conductivity $\sigma_m = 1000$ in the connected phase. The space $\mathcal{A}(\omega^*)$ is generated by piecewise linear functions as boundary data. The top row has $\alpha = 0.4$ and the bottom row has $\alpha = 0.1$. (For interpretation of the references to color in this figure legend, the reader is referred to the web version of this article.)

$$= \min_{\vec{x}\in\mathbb{R}^M} \{ \frac{\sum_{i=1}^M \sum_{j=1}^M \sum_{k=1}^N (e_i, w_k)_{\mathcal{E}(\omega^*)} (w_k, e_j)_{\mathcal{E}(\omega^*)} x_i x_j}{\|e\|^2_{\mathcal{E}(\omega^*)}} \} \tag{A.5}$$

$$= \min_{e\in V^M} \{ \frac{\sum_{k=1}^N (w_k, e)_{\mathcal{E}(\omega^*)} (w_k, e)_{\mathcal{E}(\omega^*)}}{\|e\|^2_{\mathcal{E}(\omega^*)}} \} \tag{A.6}$$

$$= \min_{e\in V^M} \{ \frac{(\mathbb{P}_{W^N} e, e)^2_{\mathcal{E}(\omega^*)}}{\|e\|^2_{\mathcal{E}(\omega^*)}} \} \tag{A.7}$$

$$= \cos^2(\beta_M^N), \tag{A.8}$$

and the identity is established.

References

[1] I. Babuška, G. Caloz, J.E. Osborn, Special finite element methods for a class of second order elliptic problems with rough coefficients, SIAM J. Numer. Anal. 31 (4) (1994) 945–981.
[2] I. Babuška, U. Banerjee, J.E. Osborn, Generalized finite element methods—main ideas, results and perspective, Int. J. Comput. Methods 1 (01) (2004) 67–103.
[3] T. Strouboulis, I. Babuška, K. Copps, The design and analysis of the generalized finite element method, Comput. Methods Appl. Mech. Engrg. 181 (1–3) (2000) 43–69.
[4] J.M. Melenk, I. Babuška, The partition of unity finite element method: Basic theory and applications, Comput. Methods Appl. Mech. Engrg. 139 (1–4) (1996) 289–314.
[5] R. Toupin, On St. Venant's principle, in: Applied Mechanics, Springer, 1966, pp. 151–152.
[6] T.Y. Hou, X.-H. Wu, A multiscale finite element method for elliptic problems in composite materials and porous media, J. Comput. Phys. 134 (1) (1997) 169–189.
[7] T. Hou, X.-H. Wu, Z. Cai, Convergence of a multiscale finite element method for elliptic problems with rapidly oscillating coefficients, Math. Comp. 68 (227) (1999) 913–943.

[8] Y.R. Efendiev, T.Y. Hou, X.-H. Wu, Convergence of a nonconforming multiscale finite element method, SIAM J. Numer. Anal. 37 (3) (2000) 888–910.
[9] I. Babuška, R. Lipton, P. Sinz, M. Stuebner, Multiscale-spectral GFEM and optimal oversampling, Comput. Methods Appl. Mech. Engrg. 364 (2020) 112960.
[10] I. Babuska, X. Huang, R.P. Lipton, Machine computation using the exponentially convergent multiscale spectral generalized finite element method, Math. Modell. Numer. Anal. M2AN 48 (2014) 493–515.
[11] I. Babuška, J.M. Melenk, The partition of unity method, Internat. J. Numer. Methods Engrg. 40 (4) (1997) 727–758.
[12] I. Babuska, R. Lipton, Optimal local approximation spaces for generalized finite element methods with application to multiscale problems, SIAM Multiscale Model. Simul. 9 (1) (2011) 373–406, http://dx.doi.org/10.1137/100791051.
[13] M.A. Schweizer, S. Wu, Evaluation of local multiscale approximation spaces for partition of unity methods, in: M. Griebel, M.A. Schweizer (Eds.), Meshfree Methods for Partial Differential Equations VIII, Springer, New York, NY, 2017, pp. 167–198, http://dx.doi.org/10.1007/978-3-319-51954-8_9.
[14] T. Strouboulis, L. Zhang, I. Babuška, Generalized finite element method using mesh-based handbooks: Application to problems in domains with many voids, Comput. Methods Appl. Mech. Engrg. 192 (28–30) (2003) 3109–3161.
[15] A. Buhr, K. Smetana, Randomized local model order reduction, SIAM J. Sci. Comput. 40 (4) (2018) A2120–A2151.
[16] K. Chen, Q. Li, J. Lu, S.J. Wright, Random sampling and efficient algorithms for multiscale pdes, SIAM J. Sci. Comput. 42 (5) (2020) A2974–A3005.
[17] Y. Evans, I. Babuska, T. Hughes, N-widths, sup-infs, and optimality ratios for the K-version of the isogeometric finite element method, Comput. Methods Appl. Mech. Engrg. 198 (2009) 1726–1741.
[18] A.L.G. Mandolesi, Grassmann angle formulas and identities, 2020, arXiv: General Mathematics.
[19] Å. Björck, G.H. Golub, Numerical methods for computing angles between linear subspaces, Math. Comp. 27 (123) (1973) 579–594.
[20] G. Dahlquist, B. Sjöberg, P. Svensson, Comparison of the method of averages with the method of least squares, Math. Comp. 22 (104) (1968) 833–845.
[21] A. Bensoussan, J.-L. Lions, G. Papanicolaou, Asymptotic Analysis for Periodic Structures, Vol. 374, American Mathematical Soc., 2011.
[22] T.J. Hughes, G.R. Feijóo, L. Mazzei, J.-B. Quincy, The variational multiscale method—A paradigm for computational mechanics, Comput. Methods Appl. Mech. Engrg. 166 (1–2) (1998) 3–24.
[23] H. Owhadi, L. Zhang, Metric-based upscaling, Commun. Pure Appl. Math.: A J. Issued Courant Inst. Math. Sci. 60 (5) (2007) 675–723.
[24] H. Owhadi, L. Zhang, Homogenization of parabolic equations with a continuum of space and time scales, SIAM J. Numer. Anal. 46 (1) (2008) 1–36.
[25] W. Hackbusch, Hierarchical Matrices: Algorithms and Analysis, Vol. 49, Springer, 2015.
[26] M. Bebendorf, Hierarchical Matrices, Springer, 2008.
[27] H. Owhadi, Bayesian numerical homogenization, Multiscale Model. Simul. 13 (3) (2015) 812–828.
[28] Y. Efendiev, V. Ginting, T. Hou, R. Ewing, Accurate multiscale finite element methods for two-phase flow simulations, J. Comput. Phys. 220 (1) (2006) 155–174.
[29] Y. Efendiev, T. Hou, Multiscale finite element methods for porous media flows and their applications, Appl. Numer. Math. 57 (5–7) (2007) 577–596.
[30] W. E, B. Engquist, X. Li, W. Ren, E. Vanden-Eijnden, Heterogeneous multiscale methods: A review, Commun. Comput. Phys. 2 (3) (2007) 367–450.
[31] W. E, P. Ming, P. Zhang, Analysis of the heterogeneous multiscale method for elliptic homogenization problems, J. Amer. Math. Soc. 18 (1) (2005) 121–156.
[32] B. Engquist, P.E. Souganidis, Asymptotic and numerical homogenization, Acta Numer. 17 (2008) 147–190.
[33] J. Nolen, G. Papanicolaou, O. Pironneau, A framework for adaptive multiscale methods for elliptic problems, Multiscale Model. Simul. 7 (1) (2008) 171–196.
[34] T. Arbogast, K.J. Boyd, Subgrid upscaling and mixed multiscale finite elements, SIAM J. Numer. Anal. 44 (3) (2006) 1150–1171.
[35] J.M. Melenk, On n-widths for elliptic problems, J. Math. Anal. Appl. 247 (1) (2000) 272–289.
[36] L. Berlyand, H. Owhadi, Flux norm approach to finite dimensional homogenization approximations with non-separated scales and high contrast, Arch. Ration. Mech. Anal. 198 (2) (2010) 677–721.
[37] H. Owhadi, L. Zhang, L. Berlyand, Polyharmonic homogenization, rough polyharmonic splines and sparse super-localization, ESAIM Math. Model. Numer. Anal. 48 (2) (2014) 517–552.
[38] T.Y. Hou, P. Liu, Optimal local multi-scale basis functions for linear elliptic equations with rough coefficient, Discrete Contin. Dyn. Syst. 36 (8) (2015) 4451–4476.
[39] K. Smetana, A.T. Patera, Optimal local approximation spaces for component-based static condensation procedures, SIAM J. Sci. Comput. 38 (5) (2016) A3318–A3356.
[40] A. Målqvist, D. Peterseim, Localization of elliptic multiscale problems, Math. Comp. 83 (290) (2014) 2583–2603.
[41] I. Babuška, U. Banerjee, Stable generalized finite element method (SGFEM), Comput. Methods Appl. Mech. Engrg. 201 (2012) 91–111.
[42] M. Griebel, M.A. Schweitzer, A particle-partition of unity method part VII: Adaptivity, in: Meshfree Methods for Partial Differential Equations III, Springer, 2007, pp. 121–147.
[43] G. Duvant, J.L. Lions, Inequalities in Mechanics and Physics, Vol. 219, Springer Science & Business Media, 2012.
[44] I. Babuška, U. Banerjee, J. Osborn, Generalized finite element methods: Main ideas, results, and perspective, Int. J. Comput. Methods 1 (2004) http://dx.doi.org/10.1142/S0219876204000083.
[45] C. Schwab, P-and Hp-Finite Element Methods: Theory and Applications in Solid and Fluid Mechanics, Oxford University Press, 1998.

[46] N. Garofalo, F. Lin, Unique continuation for elliptic operators: A geometric-variational approach, Comm. Pure Appl. Math. 40 (1987) 347–366.
[47] J.L. Kazdan, Unique continuation in geometry, Comm. Pure Appl. Math. 41 (5) (1988) 667–681.
[48] R.P. Lipton, P. Sinz, M. Stuebner, Uncertain loading and quantifying maximum energy concentration within composite structures, J. Comput. Phys. 325 (2016) 38–52.
[49] L. Borcea, Y. Gorb, Y. Wang, Asymptotic approximation of the dirichlet to Neumann map of high contrast conductive media, Multiscale Model. Simul. 12 (4) (2014) 1494–1532.